Non-methane organic gas emissions from biomass burning: identification, quantification, and emission factors from PTR-ToF during the FIREX 2016 laboratory experiment

Abigail R. Koss[1,2,3*], Kanako Sekimoto[1,2,4], Jessica B. Gilman[2], Vanessa Selimovic[5], Matthew M. Coggon[1,2], Kyle J. Zarzana[1,2], Bin Yuan[1,2,†], Brian M. Lerner[1,2,‡], Steven S. Brown[2,3], Jose L. Jimenez[1,3], Jordan Krechmer[1,3,‡], James M. Roberts[2], Carsten Warneke[1,2], Robert J. Yokelson[5], Joost de Gouw[1,2,3]

1. Cooperative Institute for Research in Environmental Sciences, University of Colorado Boulder, Boulder, CO, USA
2. NOAA Earth System Research Laboratory, Chemical Sciences Division, Boulder, CO, USA
3. Department of Chemistry, University of Colorado Boulder, Boulder, CO, USA
4. Graduate School of Nanobioscience, Yokohama City University, Yokohama, Japan
5. Department of Chemistry and Biochemistry, University of Montana, Missoula, MT, USA
* Now at Department of Civil & Environmental Engineering, Massachusetts Institute of Technology, Cambridge, MA, USA
† Now at Laboratory of Atmospheric Chemistry, Paul Scherrer Institute, Villigen, Switzerland
‡ Now at Aerodyne Research, Inc., Billerica, MA, USA

Abstract

Volatile and intermediate-volatility non-methane organic gases (NMOGs) released from biomass burning were measured during laboratory-simulated wildfires by proton-transfer-reaction time-of-flight mass spectrometry (PTR-ToF). We identified NMOG contributors to more than 150 PTR ion masses using gas chromatography (GC) pre-separation with electron ionization, H_3O^+ chemical ionization, and NO^+ chemical ionziation, an extensive literature review, and time-series correlation, providing higher certainty for ion identifications than has been previously available. Our interpretation of the PTR-ToF mass spectrum accounts for nearly 90% of NMOG mass detected by PTR-ToF across all fuel types. The relative contributions of different NMOGs to individual exact ion masses are mostly similar across many fires and fuel types. The PTR-ToF measurements are compared to corresponding measurements from open-path Fourier transform infrared spectroscopy (OP-FTIR), broadband cavity enhanced spectroscopy (ACES), and iodide ion chemical ionization mass spectrometry (I^- CIMS) where possible. The majority of comparisons have slopes near 1 and values of the linear correlation coefficient, R^2, of >0.8, including compounds that are not frequently reported by PTR-MS such as ammonia, hydrogen cyanide (HCN), nitrous acid (HONO), and propene. The exceptions include methylglyoxal and compounds that are known to be difficult to measure with one or more of the deployed instruments. The fire-integrated emission ratios to CO and emission factors of NMOGs from 18 fuel types are provided. Finally, we provide an overview of the chemical characteristics of detected species. Non-aromatic oxygenated compounds are the most abundant.

Atmospheric
Chemistry
and Physics
Discussions

36   Furans and aromatics, while less abundant, comprise a large portion of the OH reactivity. The OH reactivity,

37   its major contributors, and the volatility distribution of emissions can change considerably over the course

38   of a fire.

39   **1. Introduction**

40   Biomass burning, including wildfires, agricultural burning, and domestic fuel use, is a large source

41   of non-methane organic gases (NMOGs) to the atmosphere (Crutzen and Andreae, 1990;Akagi et al., 2011).

42   These compounds can be directly harmful to human health (Naeher et al., 2007) and contribute to the

43   formation of secondary pollutants including ozone and secondary organic aerosol (SOA) (Alvarado et al.,

44   2009;Yokelson et al., 2009;Jaffe and Wigder, 2012;Alvarado et al., 2015). Because NMOGs from biomass

45   burning are a complex mixture of many species that can change considerably depending on fuel and fire

46   characteristics, many modeling and inventory efforts have had difficulty capturing subsequent chemistry in

47   fire plumes (Alvarado et al., 2009;Grieshop et al., 2009;Wiedinmyer et al., 2011;Heald et al., 2011;Müller

48   et al., 2016;Reddington et al., 2016; Shrivastava et al., 2017). Additionally, a substantial portion of gas-

49   phase carbon may be missing from many field measurements (Warneke et al., 2011;Yokelson et al.,

50   2013;Hatch et al., 2017) and the gas phase-precursors of SOA are not sufficiently understood (Jathar et al.,

51   2014;Alvarado et al., 2015;Hatch et al., 2017). For these reasons, it is important to develop and understand

52   analytical techniques that quantify a large number of biomass burning NMOGs.

53   Gas chromatography (GC) techniques have been used to identify NMOGs emitted by biomass

54   burning in high chemical detail, and provide exact isomer identifications (Hatch et al., 2015;Gilman et al.,

55   2015;Hatch et al., 2017). However, on-line GC techniques do not provide continuous measurement and are

56   limited to certain classes of NMOGs depending on the column(s) selected and required sample

57   preconditioning steps. This makes them non-ideal for some important compounds or situations where fast,

58   continuous measurements are necessary. Whole-air sampling followed by GC can improve the time

59   resolution, but is affected by artifacts from canister storage (Lerner et al., 2017).

60   Proton-transfer-reaction mass spectrometry (PTR-MS) is a complementary technique widely used

61   in atmospheric chemistry, both standalone and with a GC interface (de Gouw and Warneke, 2007; Yuan et

62   al., 2017). This chemical ionization technique uses H_3O^+ to detect a wide range of unsaturated and polar

63   NMOGs. It can measure continuously at a very fast rate: up to 10Hz measurement has been reported in the

64   literature (Müller et al., 2010). Recently, PTR-MS instruments using time-of-flight mass analyzers (PTR-

65   ToF) with mass resolution greater than 4000 m/Δm have provided fast, simultaneous measurements of exact

66   mass and elemental formula over a wide mass range (m/z typically between 10-500 Th) with detection

67   limits in the tens to hundreds of parts-per-trillion (pptv) range (Jordan et al., 2009;Yuan et al., 2016). The

Atmospheric
Chemistry
and Physics
Discussions

68   addition of a GC interface can resolve isomers with the same elemental formula thereby providing the exact

69   identity of detected NMOGs.

70   Several recent papers have reported use of high-resolution PTR-ToF to measure biomass burning

71   NMOGs in the laboratory (Stockwell et al., 2015;Bruns et al., 2017) and the environment (Brilli et al.,

72   2014;Müller et al., 2016). The mass spectra resulting from PTR-ToF detection of biomass burning NMOGs

73   are complex, and many peak assignments are tentative. However, it is clear that PTR-ToF can provide

74   detailed NMOG measurements relevant to studying the effects of fire emissions on human health, and ozone

75   and secondary organic aerosol formation.

76   A PTR-ToF instrument (Yuan et al., 2016) was deployed during the Fire Influence on Regional and

77   Global Environments Experiment (FIREX) 2016 intensive at the US Forest Service Fire Sciences

78   Laboratory in Missoula, Montana. This experiment burned a series of natural fuels and characterized the

79   gas- and particle-phase emissions with a range of instrumentation (Selimovic et al., submitted). Aging of

80   these emissions was explored with additional chamber experiments (described elsewhere). In this paper we

81   describe the PTR-ToF instrument operation and interpretation of measurements. The focus is on direct

82   emissions. Building on work by Stockwell et al. (2015);Brilli et al. (2014), and others, we provide new,

83   more detailed, and more highly time-resolved chemistry of NMOG emissions from biomass burning than

84   previously available.

85   The purposes of this work are to improve our understanding of the complex NMOG emissions from

86   biomass burning by interpreting PTR-ToF measurements of biomass burning emissions; provide emission

87   factors and emission ratios to CO for many NMOGs; link PTR-ToF measurements to GC, Fourier-transform

88   infrared spectroscopy (FTIR), and Iodide CIMS (I$^-$ CIMS) measurements; and report instrument operation

89   and data quality assurance information that will support future analyses. Novel tools to study NMOGs

90   measured by PTR-ToF applied in this work include (1) use of a GC interface to provide an additional level

91   of chemical information; (2) use of NO$^+$ CIMS (switchable-reagent-ion) chemistry to support compound

92   identification; and (3) use of an improved method to estimate the instrument sensitivity to NMOGs not

93   directly calibrated.

94   **2. Methods**

95   **2.1 Fire Sciences Laboratory experimental setup**

96   Controlled biomass combustion experiments were conducted in a large (12.5m × 12.5m × 22m

97   high) indoor facility at the US Forest Service Fire Sciences Laboratory. Fuels were burned underneath a

98   1.6m diameter exhaust stack. Emissions were vented through the stack to 17m height, where a sampling

99   platform is located. The pressure, temperature, and relative humidity of the air in the combustion chamber

Atmospheric
Chemistry
and Physics
Discussions
Open Access

EGU

100   were monitored and low light conditions were present during experiments. The Fire Sciences Laboratory

101   facility is described in more detail elsewhere (Christian, 2003, 2004;Burling et al., 2010;Stockwell et al.,

102   2014). The FIREX 2016 intensive burned fuels characteristic of the western US, including Ponderosa pine,

103   Lodgepole pine, Douglas fir, Engelmann spruce, subalpine fir, manzanita, chamise, sage, and juniper.

104   Several other types of fuels were also burned, but with fewer replicates, and these included additional pine

105   species (Loblolly and Jeffrey pine), bear grass, rice straw, ceanothus, dung, peat, excelsior, and commercial

106   lumber. Experiments with western fuels included combustion of both specific components of the fuel, such

107   as canopy, litter, and duff, and more realistic burns that included a mix of components (Selimovic et al.,

108   submitted).

109   Two types of combustion experiments were conducted. In the first set of experiments, the "stack

110   burns", emissions were entrained into the ventilation stack and measured from the 17m sampling platform.

111   These experiments allowed characterization of changes in emission composition during the course of a fire

112   and typically lasted five to twenty minutes. In the second set of experiments, the "room burns", emissions

113   were not vented and were allowed to mix and fill the combustion chamber. These experiments lasted several

114   hours and provided a more compositionally stable mixture for instruments requiring a longer sampling time.

115   In this work, we discuss 58 stack burns measured directly with PTR-ToF, and these data were used for the

116   comparison between instruments. We also reference measurements from an additional seven stack burns

117   measured directly with NO^+-CIMS, and discuss results from three stack burns and three room burns that

118   were measured with GC-PTR-ToF, using both H_3O^+ and NO^+ reagent ion chemistry. Because there was not

119   a clear temporal separation between fire processes, and because some compounds were lost to the chamber

120   walls (Stockwell et al., 2014), room burns measured directly with PTR-ToF were not used for compound

121   identification and calculation of emission factors.

2.2 Instrumentation

123   An overview of the instruments referenced in this work is given in Table 1.

2.2.1 PTR-ToF and NO^+-CIMS

125   The PTR-ToF is a chemical ionization mass spectrometer typically using H_3O^+ reagent ions. Trace

126   gases with a proton affinity higher than that of water are protonated in a drift tube region, and are detected

127   sensitively with typical detection limits in the tens to hundreds of parts-per-trillion (pptv) range for a 1-sec

128   measurement time. The main advantages of this technique are a response to a wide range of polar and

129   unsaturated NMOGs, a low degree of fragmentation, and fast, on-line measurement capability. PTR-ToF

130   additionally detects several inorganic species, including ammonia (NH_3), isocyanic acid (HNCO), hydrogen

131   sulfide (H_2S), and nitrous acid (HONO), which are included in our discussion of NMOGs.

Atmospheric
Chemistry
and Physics
Discussions

132   The instrument used in this work is very similar to that described by Yuan et al. (2016), with two

133   relevant differences. The PTR-ToF instrument described by Yuan et al. (2016) includes two RF-only

134   segmented quadrupole ion guides between the drift tube and time-of-flight mass analyzer; while the current

135   version has only one ion guide. The effects of this are that the sensitivities are slightly higher (~25% on

136   average), low ion masses (<m/z 40 Th) are transmitted with higher efficiency, and the humidity dependence

137   of NMOG sensitivity is less severe. There is also a higher flow rate (150 sccm) into the drift tube. Second,

138   the instrument inlet (held at 40°C) consists of 1/16" ID PEEK tubing rather than 1/8" PFA, which reduced

139   residence time in the inlet.

140   The PTR-ToF is equipped with a switchable reagent ion source that allows for H_3O^+ and

141   alternatively NO^+ ionization, by flowing either water vapor for H_3O^+ or ultrapure air for NO^+ through a

142   hollow cathode ion source and adjusting ion source and ion guide voltages. NO^+ chemical ionization of

143   NMOGs creates different product ions than H_3O^+ chemical ionization, and the ionization mechanism

144   depends on functional group (Koss et al., 2016). The PTR-ToF instrument in NO^+ configuration (NO^+-

145   CIMS) can therefore detect several additional classes of NMOGs (e.g. branched alkanes) and can

146   differentiate some sets of isomers, such as aldehydes and ketones, and nitriles and pyrroles. NO^+-CIMS is

147   described in detail by Koss et al. (2016). The NO^+-CIMS was used to measure emissions directly, from a

148   small number of coniferous fuels, and as the detector for the GC instrument, for several fuel types.

149   In H_3O^+ mode the PTR-ToF was operated with an electric field to number density ratio (E/N) of

150   120×10^{-17} V cm^2 (= 120 Townsend or Td). Measurements were made at 2Hz frequency. Ion m/z from 12-

151   500 Th were measured, and 12-217 Th were quantified with a maximum resolution of 4500 FWHM m/Δm.

152   This is sufficient to resolve many isobaric species, but many peaks still overlap in the mass spectrum.

153   Overlap of an ion peak by an intense neighbor can strongly affect the accuracy of that ion measurement,

154   and such affected ions were excluded from further analysis. ToF data were analyzed using the Tofware

155   software package (Aerodyne Research Inc./ Tofwerk AG). For approximately one-half of the stack

156   experiments, NMOG ion concentrations were temporarily high enough to deplete the reagent ion by 10-

157   50%. Under these conditions, sensitivity to NMOGs is lower and nonlinear (Veres et al., 2010b). We

158   corrected NMOG ion signals for this effect, although effects from secondary proton-transfer reactions could

159   still be a significant source of inaccuracy (Section S1). Raw ion count rates (counts-per-second, cps) were

160   corrected for duty-cycle discrimination in the ToF extraction region, and normalized to the intensity of the

161   reagent ion (H_3O^+ 10^6 cps or NO^+ 10^6 cps). Correction for humidity effects and conversion of ion signal to

162   mixing ratio are discussed in Section 2.3. Before each fire, we first measured instrument background by

163   passing air from the combustion chamber through a heated platinum catalyst, then measured chamber

164   background. Concentrations of NMOGs during the fire were generally several orders of magnitude higher

165   than either background.

Atmospheric
Chemistry
and Physics
Discussions

166   The NO^+-CIMS/PTR-ToF transfer inlet was ½" OD (3/8" ID) PFA, heated to 40°C, with a flow

167   rate of 100 SLPM. It was 16m long (residence time 0.7 seconds) and located on the sampling platform for

168   stack burns, and 7m long (residence time 0.3 seconds) and located 3m above the combustion chamber floor

169   for room burns. The instrument subsampled 500 sccm through a 40°C 10 cm 1/16" ID PEEK capillary

170   orthogonally via PFA branch reducing tee mounted to the main inlet. Most particles were separated from

171   the CIMS subsample capillary through virtual impaction, although a small, unquantified amount of

172   particulate matter did enter the smaller instrument inlet.

173   NMOGs could be lost to transfer inlet, instrument tubing, or drift tube surfaces. Based on good

174   agreement with instrumentation on the sampling platform (Section 3.3.1) inlet losses of highly volatile

175   compounds were negligible, but we were not able to quantify possible losses of less volatile compounds.

176   Measurement of compounds with saturation vapor pressure (C_0) less than 10^5 µg m^{-3} may be affected

177   (Pagonis et al., 2017). Slight delay in the instrument response to some compounds with C_0 close to 10^4 µg

178   m^{-3} was observed.

179   2.2.2 GC-MS and GC-PTR-ToF

180   The gas chromatograph (GC) instrument cryogenically pre-concentrates 4-minute samples of

181   NMOGs before separation on one of two capillary columns (Lerner et al., 2017). The sample stream is

182   separated into two channels that are optimized to reduce water and carbon dioxide before cryogenic trapping

183   of NMOG. The first channel (trapping at -165 ºC) is connected to an Al_2O_3/KCl PLOT column optimized

184   for C_2-C_6 hydrocarbons. The second channel (trapping at -135 ºC) uses a medium polarity polysiloxane

185   (MXT-624) column optimized for C_6-C_{10} hydrocarbons and many polar compounds. The two channels are

186   analyzed sequentially.

187   The eluent from the GC columns was directed to either an electron ionization (EI) quadrupole mass

188   spectrometer (Agilent model 5975C) or to the PTR-ToF. The quadrupole mass spectrometer has unit mass

189   resolution and was operated in full ion scan mode, from m/z 19 to 150 Th. When the PTR-ToF, in either

190   H_3O^+ and NO^+ configuration, was used as the detector, the 2 sccm eluent from the columns was introduced

191   directly into the drift tube. To maintain pressure (2.4 mbar) in the drift tube, an additional 50 sccm of

192   catalyst-generated clean air was added to the drift tube. This is lower than the 150 sccm of flow used during

193   non-GC-PTR-ToF operation but does not affect compound identification.

194   The GC inlet for stack burns was ½" OD PFA, 16m long, located on the sampling platform, with a

195   continuous flow rate of 20 lpm. A subsample was directed to the instrument with a ¼" OD PFA, 2m long

196   line with flow rates from 2-7 lpm. For room burns the inlet was ¼" OD PFA, 7m long, and located 3m

197   above the combustion chamber floor. A flow rate of 2-7 SLPM was used. For both stack and room burns

Atmospheric
Chemistry
and Physics
Discussions
Open Access
EGU

198   the inlet was heated to 40°C and the stream was dynamically diluted with humidified UHP N_2 (1 to 3 parts

199   smoke to 5 parts N_2). Particles were reduced by virtual impaction.

200   Two stack experiments (both Douglas fir) were measured with both GC-EI-MS and GC-PTR-ToF;

201   one stack experiment (Englemann spruce duff) and three room experiments (Douglas fir, Subalpine fir, and

202   sage) were each measured with GC-EI-MS, GC-PTR-ToF, and GC-NO$^+$-CIMS. Two additional samples

203   (of a room burn of sage), one with H_3O^+ and one with NO$^+$ chemistry, were analyzed using an accelerated

204   GC temperature ramp program to better observe late-eluting compounds. Each four-minute sample was

205   analyzed with just one type of detector, and the detector was switched for the next four-minute sample. For

206   room experiments and duff stack burns, NMOG composition was largely consistent between successive

207   four-minute GC samples. Other stack burns varied more quickly. The room experiment GC-CIMS analyses

208   detected NMOGs more sensitively because we were better able to adjust the GC sample stream dilution.

209   Finally, we measured a 56-component NMOG calibration standard with the GC-PTR-ToF and GC-NO$^+$-

210   CIMS (three replicates) to help establish GC retention times.

211   **2.2.3 Other instrumentation**

212   A number of trace gases measured by the PTR-ToF were also measured by other instruments (Table

213   1), and in Section 3.3 we compare these measurements. The OP-FTIR instrument was located on the

214   sampling platform with the optical path spanning the stack, and therefore did not have an inlet (Stockwell

215   et al. 2014). The OP-FTIR employed a time resolution of 1.37 seconds and the PTR-ToF data were

216   interpolated to the OP-FTIR sampling times for the intercomparison.

217   Glyoxal, methylglyoxal and HONO were measured with the NOAA Airborne Cavity Enhanced

218   Spectrometer (ACES) instrument, which uses broadband cavity enhanced spectroscopy. Wavelength

219   resolved gas-phase extinction was measured in two spectral regions, one in the UV (361 nm to 390 nm) and

220   one in the blue (438-468 nm), and then fit using literature cross sections to retrieve the concentrations of

221   NO_2, HONO, methylglyoxal, and glyoxal (Min et al., 2016). Data from this instrument were reported at 1-

222   second intervals. The ACES instrument inlet was located on the sampling platform, with an inlet of

223   approximately 1m length sampling from the center of the stack flow directly above the OP-FTIR optical

224   path.

225   The I- CIMS chemically ionizes organic and inorganic gases through iodide adduct formation, and

226   analyzes the resulting ions with a high-resolution time-of-flight mass spectrometer (Lee et al., 2014). The

227   I$^-$ CIMS instrument shared an inlet with the PTR-ToF. Air was subsampled from this inlet and dynamically

228   diluted with UHP N_2 to prevent reagent ion depletion. The dilution factor was determined by comparing the

229   CO_2 concentration before and after dilution measured by a LICOR LI6252 co-located with the I$^-$ CIMS. I$^-$

230   CIMS calibration factors were determined by direct calibration for the species discussed here.

2.3 Calibrations and method for estimating calibration factors

The calibration factor (units of ncps/ppbv) is the normalized counts per second (ncps) per ppbv of the NMOG(s) whose PTR product is that ion. The ncps are derived from the raw ion count rate (counts per second, cps), corrected for the mass-dependent duty-cycle of the ToF extraction, and normalized to the detected ion count rate of the primary ion (H_3O^+ cps $\times 10^{-6}$). We detect 8.5-11.5$\times 10^6$ H_3O^+ ions per second. We detect about 1000 cps/ppbv of acetone and 650 cps/ppbv of benzene. We provide the sensitivity here as raw ion count rate to enable comparison to other PTR-MS instruments, which may have different detected intensity of H_3O^+. This is about an order of magnitude higher than similar generation commercially available PTR-ToF (Jordan et al., 2009), but an order of magnitude lower than new PTR-ToF instruments that use a different drift tube design (Breitenlechner et al., 2017). Calibration factors in this work were obtained by (1) direct calibration, (2) calculation using kinetic rate constants (Sekimoto et al., 2017a), or (3) comparison with OP-FTIR, which will be discussed in section 3.3. Calibration factors for all ion masses are provided in Table S1.

The calibration factors of 37 species were determined experimentally by introducing a known concentration of a NMOG from a standard cylinder, a permeation source (Veres et al., 2010a), a diffusion cell for isocyanic acid and methyl isocyanate (Roberts et al., 2010), or a liquid calibration unit (Ionicon Analytik). The calibration factors of these species have an error of 15% (details in Table S1).

It is unrealistic to experimentally determine calibration factors for all NMOG species detected in biomass burning. Many compounds are highly reactive and cannot be purchased from a commercial supplier. Several methods to estimate calibration factors have been previously used by PTR-MS operators. For example, both Warneke et al. (2011) and Stockwell et al. (2015) estimated calibration factors for uncalibrated species based on ion mass to charge ratio and chemical formula in the latter case.

Sekimoto et al. (2017a) recently developed an improved method of estimating calibration factors. The instrument calibration factor is linearly proportional to the kinetic capture rate constant of the H_3O^+ proton transfer reaction, with additional corrections for mass-dependent transmission and NMOG ion fragmentation, both of which can be constrained experimentally. The proportionality is determined by direct calibration of a small subset of NMOGs. For this work, we used a calibration gas standard containing acetonitrile, acetaldehyde, acetone, isoprene, 2-butanone (methyl ethyl ketone, MEK), benzene, toluene, o-xylene, and 1,2,4-trimethylbenzene dynamically diluted to 1-10 ppb. The kinetic capture rate constant can be calculated using the polarizability and permanent dipole moment of the NMOG or alternatively for unidentified ions using the NMOG molecular mass and elemental composition. Figure 1 compares the measured and calculated calibration factors for several compounds. Most calculated calibration factors (72%) fall within +10/-50% of the measured sensitivity. The calculated calibration factor provides the upper limit to the sensitivity, and some of the measured calibration factors are lower than predicted. These

Atmospheric
Chemistry
and Physics
Discussions

265 typically include species with proton affinity close to water (e.g. formaldehyde) and species that fragment

266 to small masses (e.g. ethanol). A detailed discussion of why measured calibration factors can deviate from

267 calculated ones is given in Sekimoto et al. (2017a).

268 If an identified ion mass has only one NMOG contributing, as is the case for 65% (102) of the ion

269 masses with signal in the fire, we used the calibration factor from direct calibration or the Sekimoto et al.

270 (2017a) method. If an identified ion mass has more than one NMOG contributing, we used a weighted

271 average of the calibration factors of all NMOG contributors to this ion mass (Eq. 1). The determination of

272 relative NMOG contributions to the total ion signal of each individual mass was based on GC-PTR-ToF

273 measurements, comparisons to other instruments, time-series analysis, and reported values from literature

274 and will be described in Section 3.

275 $$cal\ factor_{average} = \left(\sum_i \frac{contribution_i}{cal\ factor_i} \right)^{-1} \qquad \text{Eq. 1}$$

276 The uncertainty for calibration factors for identified NMOGs ranges from 15% to 50% depending

277 on the calibration method used (Table S1). For ion masses for which we were not able to propose a NMOG,

278 a calibration factor was estimated based on the elemental composition of the ion mass (Sekimoto et al,

279 2016a). The uncertainty for calibration factors for unidentified species is within 10% higher to 50% lower.

280 Ambient humidity can change the measured sensitivity of a NMOG species (Yuan et al., 2016).

281 For species whose calibration factor was measured, a humidity correction factor was also experimentally

282 determined. We currently have no method to predict the humidity dependence of the sensitivity for other

283 species, so for all other species no humidity correction was applied. To minimize the error from this

284 omission, we calibrated compounds that were abundant in emissions and that likely have strong humidity

285 dependence. These include compounds with proton affinities close to water (e.g. HNCO) and compounds

286 whose ionization mechanism includes loss of water (e.g. 1-propanol). Excluding these compounds, the

287 average measured humidity correction factor was less than 15% for the highest humidity conditions

288 experienced during FIREX (18 g/kg). Measured sensitivities of different NMOGs both increased and

289 decreased with humidity and an unknown humidity correction will likely only cause a small bias for total

290 NMOG signals. There were no systematic differences in humidity between fires of different fuels.

291 **3. Results & discussion**

292 **3.1 Identification of PTR-ToF ion masses**

293 During the Fire Lab experiments we measured 574 ions that were enhanced in emissions from one

294 or more fuel types. Of these, we identified 156 ion masses with a high degree of certainty and for which a

295 calibration factor can be determined. An additional 12 ion masses were identified as fragments of one or

296 more NMOGs whose main product ion was already included in the list of 156 ions. Finally, 4 ions were

297   identified as being a common product of a large number of structurally dissimilar NMOGs. These 172 ions,

298   their identification, and support for that identification are listed in Table S1. Table S1 provides detailed

299   information on the isomer contributions to each mass, sensitivities and calibration uncertainty, literature

300   references, GC measurements, and observations from time series correlations. Table S1 additionally

301   includes quantitative information on OH rate constants, instrument intercomparisons, and NO^+-CIMS ion

302   mass identifications. These 172 masses represent about 95% of the total signal (ncps) from m/z 12-217 Th

303   measured by PTR-ToF. Below, we describe the methods used to ascribe NMOG identifications to PTR-

304   ToF ion masses.

305   **3.1.1 Literature survey**

306   Identifications of many NMOGs emitted from biomass burning have been previously reported,

307   using GC, PTR-MS, and optical methods. We compiled a list of observed NMOGs and identifications to

308   use as a starting point. The papers we referenced included Karl et al. (2007), Warneke et al. (2011), Brilli

309   et al. (2014), Stockwell et al. (2015), Müller et al. (2016), and Bruns et al. (2017), which focus on PTR-MS

310   measurements, and Gilman et al. (2015), Hatch et al. (2015), and Hatch et al. (2017), which focus on GC

311   measurements. Gilman et al. (2015) used 1D-GC and focused on the most volatile species, and Hatch et al.

312   (2015) and Hatch et al. (2017) used 2D-GC and included many additional less volatile species. NMOG

313   emission factors of identified compounds and the estimated mass of unidentified species have been

314   reviewed by fire/ecosystem type globally (e.g. Akagi et al. (2011);Yokelson et al. (2013)), but significant,

315   recent measurements have not yet been included in the on-line updates: e.g. (Hatch et al., 2017). Finally,

316   for some compounds, we referenced studies of pyrolysis products of lignin, cellulose, and hemicellulose,

317   which used GC-MS, X-ray spectroscopy, FTIR, theoretical calculations, and other analytical methods to

318   identify major products and common reaction pathways (Patwardhan et al., 2009;Lu et al., 2011;Zhang et

319   al., 2012; Heigenmoser et al., 2013;Collard and Blin, 2014; Liu et al., 2017a).

320   We assessed each identification as strongly or weakly supported. Strong identifications include

321   those reported by many separate studies, NMOGs identified using GC methods (especially 2D-GC-ToF-

322   MS), and those supported by evidence from pyrolysis or other literature. Weak identifications include those

323   with disagreement between different studies, tentative identifications based on only mass-to-charge ratio or

324   elemental formula, and identifications that are inconsistent with reported formula or that are chemically

325   implausible (e.g. highly strained structure). Identifications from literature and citations are listed in Table

326   S1. Overall we found literature evidence for 68% of our ion identifications. Our interpretation differs from

327   previously published PTR-MS interpretations for 34 ion masses as noted in Table S1. Forty-eight ion

328   masses have not been previously reported in PTR-MS measurements of biomass burning.

Atmospheric
Chemistry
and Physics
Discussions

3.1.2 GC-PTR-ToF measurement

329

330   Using gas chromatographic separation before measurement with PTR-MS is a powerful tool that

331 has been widely used in many environments (Warneke et al., 2003;Karl et al., 2007;Warneke et al.,

332 2011;Yuan et al., 2014). The combination of measured chromatographic retention time and product ions

333 with GC-PTR-ToF, GC-NO$^+$-CIMS, and GC-EI-MS allows the unambiguous identification of the various

334 isomers contributing to the PTR-ToF signal of many ions. Some additional ion masses had high signal in

335 direct measurement of fire emissions, but did not appear in any chromatographs. This also provides insight

336 into the NMOG chemical structure, as certain functional groups, like acids, cannot travel through the GC

337 system. An example of GC-PTR-ToF measurement is shown in Fig. 2. Panel A in this figure shows the

338 dense chromatographic elution of hundreds of peaks over the 800-second elution period. These

339 chromatographic peaks are detected on several hundred PTR ions. Panel B shows the measured intensity

340 of m/z 68.050 $C_4H_5NH^+$ during a 280-second segment of the elution, which includes product ions from

341 pyrrole and several butene nitriles. Panel C shows the same 280-second retention-time period, from a

342 sample taken immediately after the one shown in Panel B, but measured with NO$^+$-CIMS. These isomers

343 can be distinguished by comparing GC-PTR-ToF and GC-NO$^+$-CIMS chromatography, as NO$^+$ reacts with

344 pyrrole but not nitriles.

345   The relative intensities of the eluted peaks were used to quantify the relative contribution of each

346 NMOG to each ion mass. The size of a chromatographic peak is determined not only by the mixing ratio

347 of that NMOG in ambient air and the mass spectrometer response, but also by the trapping and elution

348 efficiencies of the GC pre-separation unit. As isomers have the same molecular weight and elemental

349 composition, their volatilities and trapping efficiencies are generally similar. For example, pyrrole and 3-

350 butene nitrile have similar vapor pressures of 1.1 and 2.5 kPA at 25ºC, compared to ethane (4000 kPA) and

351 1,4-diethylbenzene (0.13 kPA) which are the most and least volatile species measured by the GC,

352 respectively (values from CRC Handbook, 97th ed). Here we assumed that all compounds that create the

353 same PTR ion mass have similar GC trapping efficiencies. This assumption is supported by GC-PTR-ToF

354 measurements of C4-alkenes, C5-alkenes, C8-aromatics, and C9-aromatics in the 56-component NMOG

355 GC calibration standard. These isomer groups have equal concentrations in the calibration gas and their

356 resulting GC-PTR-ToF chromatographic peaks had similar areas.

357   The same GC methods were used to identify some signals from the NO$^+$-CIMS. Observed and

358 identified NO$^+$-CIMS ion masses are included in Table S1. Hundreds of carbon-containing ion masses are

359 also present in a typical NO$^+$-CIMS mass spectrum. Using GC-NO$^+$-CIMS, we identified the NMOG

360 contributors to an average (across all fires measured with NO$^+$-CIMS) of 32% of the total signal of these

361 ions. More identifications could likely be made by analysis with other techniques (intercomparisons, time-

Atmospheric
Chemistry
and Physics
Discussions

362   series correlations, literature review, etc.) but were not attempted here. The NO$^+$-CIMS ion mass

363   identifications are included here as a reference for future work, but are not discussed further.

3.1.3 Time-series correlation

365   Some species measured by the PTR-ToF have several possible isomers, have not been previously

366   reported in the literature, and are not transmittable through the GC. The identifications of these compounds

367   are less certain. For these, we selected several reasonable isomeric structures based on the types of

368   compounds typically seen in biomass burning emissions: substituted furans and aromatics, nitriles,

369   pyridines, terpenes, and carbonyls. Then, we compared the temporal profile of these ion signals during

370   several fires to compounds with more certain identification. Compounds with similar structure and

371   functionality likely have similar behavior. Dissimilar compounds can also sometimes have similar temporal

372   profiles (Yokelson et al., 1996), but it is still likely that time series correlation points to the correct

373   assignment or a species with similar chemical functionality as the true assignment.

374   An example of how time-series correlation is used to identify a species is shown in Fig. 3. m/z

375   115.039 Th C$_5$H$_4$O$_3$H$^+$ is the unidentified species, for which there is no strong literature or GC evidence.

376   This formula has several plausible isomers, including furan alcohols (e.g.

377   dihydro(hydroxymethyl)furanone) and methyl-dihydrofurandione. Several other furan alcohols have been

378   unambiguously identified, including 2-furanmethanol (from GC-PTR-ToF) and 2,5-

379   (hydroxymethyl)furfural (reported in pyrolysis literature, Lu et al. (2011)). Dihydrofurandione has also

380   been identified (limited isomeric possibilities). Comparing the time series of these species during a stack

381   experiment fire shows that m/z 115.039 C$_5$H$_4$O$_3$H$^+$ correlates better with furan alcohols than with

382   dihydrofurandione. Thus m/z 115.039 is more likely to be a furan alcohol. Based on structural similarity

383   and reported pyrolysis pathways that frequently produce 2,5- substituted furans (Collard and Blin, 2014),

384   dihydro-5-(hydroxymethyl)-2[3H]-furanone is a likely compound.

3.2 NMOG ion speciation for different fuel types and fire conditions

386   As shown in the supplemental information, the contribution of isomers to any particular PTR ion

387   exact mass was consistent between the four fuels (Douglas fir, Engelmann spruce duff, Subalpine fir, and

388   sage) sampled with GC-PTR-ToF. Comparing all GC-PTR-ToF samples, the isomeric speciation on a

389   particular exact mass typically varied by only 11% (the standard deviation of the contribution of each isomer

390   to total signal on that mass) and therefore the same study-average NMOG contributions to each ion exact

391   mass were used for all fuel types, whether or not supporting GC information was available. This is similar

392   to the variation of isomer speciation reported by Hatch et al. (2015) (5% on average), who investigated six

393   diverse fuel types. Compounds that had larger variability between GC-PTR-ToF samples (and between fuel

Atmospheric
Chemistry
and Physics
Discussions
Open Access
EGU

394   types) include m/z 67.054 $C_5H_6H^+$ (cyclopentadiene), which has substantial and variable interference from

395   an isoprene fragment; and m/z 153.127 $C_{10}H_{16}OH^+$, which consists mainly of camphor in sagebrush fires,

396   and of other oxygenated monoterpenes in fires of other fuels. Additionally, in burns of ceanothus, which

397   was not sampled with GC-PTR-ToF, m/z 133.065 $C_9H_8OH^+$ was enhanced, did not correlate as well with

398   benzofuran (m/z 119.049 $C_8H_6OH^+$) and may include a contribution from another isomer such as

399   cinnamaldehyde.

400   The instantaneous speciation of isomers may also change over the course of a fire, especially as the

401   fire shifts between various higher and lower temperature chemical processes. We used time-series

402   correlation to identify several masses that may have variable NMOG contributors. This analysis was done

403   on Fire 02, which burned representative Ponderosa Pine forest-type fuels. This fire was selected because

404   Ponderosa Pine was the most comprehensively measured fuel type during the FIREX 2016 experiment, this

405   particular fire had distinctly different NMOG speciation at the beginning (higher temperature) and end

406   (lower temperature) of the fire, and reagent ion depletion did not affect the results.

407   We identified three ions with high signal whose NMOG contributors may be substantially different

408   between high- and low-temperature processes in a fire: m/z 109.065 $C_7H_8OH^+$, which likely includes more

409   2-methylphenol from high-temperature processes and more anisol from lower temperature processes; m/z

410   112.039 $C_5H_5NO_2H^+$, which likely includes a greater contribution from methyl maleimide in high

411   temperature processes and more dihydroxy pyridine from low temperature processes; and m/z 123.080

412   $C_8H_{10}OH^+$, which likely includes more C2-phenols from high temperature processes and more methylanisol

413   from low temperature processes (similar to m/z 109). Time series comparisons are shown in Fig. S2.

414   These three pairs of identifications in Fig. S2, and their relative contributions to total ion signal,

415   are not well constrained. An additional instrument technique, such as a fast GC capable of separating

416   substituted furans and aromatics, or a better understanding of I⁻ CIMS chemical specificity and more

417   accurate calibration on both instruments, would be helpful. To convert instrument signal (ncps) of these

418   ions to mixing ratio, we applied the average calibration factor of the two isomers.

419   **3.3 Intercomparison with other instruments**

420   Several species detected by the PTR-ToF were also measured by other instruments (details in Table

421   1). The intercomparison is summarized in Fig. 4. All slopes shown in the figure and discussed in the text

422   are the orthogonal distance regression (ODR) slope of H_3O^+-CIMS to the other instrument; R^2 values are

423   from vertical distance regression of PTR-ToF against the other instrument. The scatter plots are shown in

424   Figures S3-S5.

3.3.1 Comparison with OP-FTIR

Fifteen species were compared between the PTR-ToF and FTIR. Methanol, formaldehyde, formic acid, propene, acetic acid, ethene, acetylene, furan, phenol, and furfural were calibrated directly on the PTR-ToF and have uncertainty of 15%. For HONO, HCN, and ammonia, we were not able to determine a calibration factor directly and so we set the calibration factors equal to the slope of the comparison between the FTIR and PTR-ToF during Fire 72 (Ponderosa pine with realistic fuel mixture, selected for early data availability, long burning time of 30 minutes, and mix of flaming and smoldering conditions). Glycolaldehyde was calibrated using the method from Sekimoto et al. (2017a) with an uncertainty of 50%; the PTR-ToF measurement of m/z 61.028 $C_2H_4O_2H^+$ (sum of glycolaldehyde and acetic acid) has an uncertainty of 27%. FTIR hydroxyacetone was compared to PTR-ToF m/z 75.044 $C_3H_6O_2H^+$, which was calibrated using the Sekimoto et al. (2017a) method and is the sum of methyl acetate (estimated 37% of mixing ratio), ethyl formate (14%), and hydroxyacetone (48%), with uncertainty 50%. 1,3-butadiene was calibrated with the Sekimoto et al. (2017a) method and has an uncertainty of 50%. The method from Sekimoto et al. (2017a) provides the lower bound of concentration.

Methanol has agreed within stated uncertainties between PTR-MS and FTIR in several previous studies (Christian, 2004;Karl et al., 2007;Warneke et al., 2011;Stockwell et al., 2015), and this work shows an average slope of 0.99 and R^2 of 0.95. The comparison of formaldehyde between PTR-ToF and FTIR has an average slope = 1.1 and average R^2= 0.94, which is consistent with the comparison shown in Warneke et al. (2011). Other compounds that compare within the stated uncertainty in slope and have correlation coefficient >0.8 are ammonia, the sum of acetic acid and glycolaldehyde (compared to PTR-ToF m/z 61.028 $C_2H_4O_2H^+$), formic acid, HONO, acetylene, propene, and HCN. Based on the comparison with FTIR, the PTR-ToF 3σ LoD for HONO is about 9.5 ppbv, which is likely not sufficient to measure HONO in ambient air except in the most highly concentrated, fresh biomass burning plumes.

The high degree of correlation between PTR-ToF and FTIR for acetylene and ethene is notable, because these two compounds cannot be ionized by proton transfer from H_3O^+ as their proton affinities are too low. The detected NMOG product ions (acetylene, at m/z 26.015 $C_2H_2^+$) and ethene (m/z 28.031 $C_2H_4^+$) are most likely the product of charge transfer from contaminant O_2^+ from the ion source, which was high at 12% of H_3O^+ during this experiment. The acetylene comparison has a higher degree of scatter ($R^2 = 0.83$), which is likely an effect of interferences from fragments of other species as identified by GC-PTR-ToF. Ethene has better correlation ($R^2 = 0.94$); from the GC-PTR-ToF we observed that m/z 28.031 $C_2H_4^+$ is specific for ethene. The disagreement in slope may be due to variability in O_2^+.

Other compounds including 1,3-butadiene, furan, hydroxyacetone, phenol, and furfural, agreed within a factor of two (slopes of 1.6, 1.5, 0.6, 0.7, and 0.6, respectively) and average R^2 values <0.8. These species were often near the 0.73 Hz detection limit of the OP-FTIR and the discrepancy in slopes and low

Atmospheric
Chemistry
and Physics
Discussions

459   correlation coefficients are likely an effect of including this data in the intercomparison. Emission ratios

460   and emission factors (EF) are based on fire-integrated excess values that benefit from significant signal

461   averaging. Many of the above species have EF that agree between PTR-ToF and FTIR within 10%

462   (Selimovic et al., submitted; Table S1). Additionally, it has been shown that the FTIR fire-integrated

463   emission factors derived for hydroxyacetone is in excellent agreement to that reported for real wildfires by

464   Liu et al., (2017b) (Selimovic et al., submitted).

465   **3.3.2 Comparison with ACES**

466   Three species were compared between the PTR-ToF and ACES: HONO, glyoxal, and

467   methylglyoxal. HONO agrees with an average slope of 1.13 and R^2=0.95. Since the PTR-ToF sensitivity

468   factor for HONO was determined by comparison to FTIR, this slope indicates the agreement between FTIR

469   and ACES. Methylglyoxal has a slope of 0.42 and R^2=0.85. The poorer agreement for methylglyoxal is

470   probably due to interferences on both instruments. The PTR-ToF measures both methylglyoxal and acrylic

471   acid at m/z 73.028 $C_3H_4O_2H^+$; both were calibrated using the Sekimoto et al. (2017a) method. The

472   calculation has uncertainty of 50% and gives the lower bound of concentration. The ACES instrument

473   measures a series of substituted α-dicarbonyls, including 2,3-butadione, from a relatively diffuse absorption

474   band that is common to these species. Development of a specific measurement for methyl glyoxal is a target

475   of future research, because this compound is an important SOA precursor whose emission from biomass

476   burning has not been well constrained (Hays et al., 2002;Fu et al., 2008). The methylglyoxal measurement

477   may be improved with changes to the ACES resolution and spectral correction routines.

478   The comparison of glyoxal is similarly poor (slope =2.56 and $R^2 = 0.64$). This is probably because

479   of incomplete resolution of m/z 59.013 $C_2H_2O_2H^+$ from m/z 59.049 $C_3H_6OH^+$ (acetone), which is a very

480   large neighboring peak in the PTR-ToF mass spectrum. Poorly resolved peaks such as glyoxal are normally

481   not reported (Section 2.2.1). PTR-MS has been shown to have low sensitivity to glyoxal (LoD=250-700

482   pptv), with strong humidity dependence, and can be easily lost on inlet surfaces (Stönner et al., 2017).

483   Additionally, the PTR-ToF glyoxal sensitivity was calculated and has an uncertainty of 50%. The glyoxal

484   measurement may be significantly improved with better PTR-ToF sensitivity and mass resolution.

485   **3.3.3 Comparison with I⁻ CIMS**

486   Some data were compared to I⁻ CIMS for one fire (Fire 72, Ponderosa pine with realistic blend of

487   fuel); a more detailed comparison will require significant additional analysis of the I⁻ CIMS data set.

488   Although many ion masses overlap between the PTR-ToF and I⁻ CIMS, we selected seven that have

489   straightforward interpretation on both instruments: HCN, formic acid, phenol, vanillin, acetic acid and

490   glycolaldehyde, acrylic acid and methylglyoxal, and cresol and anisol. These compounds were all directly

491   calibrated on the I- CIMS, with an uncertainty of ±15%. Formic acid, phenol, vanillin, acetic acid, cresol,

492   and anisol were calibrated directly on the PTR-ToF, and the HCN sensitivity was taken from the comparison

493   to FTIR. Glycolaldehyde, acrylic acid, and methylglyoxal were calibrated using the Sekimoto et al. (2017a)

494   method with an uncertainty of 50%. The comparison for HCN, formic acid, and phenol is excellent (slopes

495   = 0.97, 0.94, and 1.08; R^2=0.99, 0.99, 0.98, respectively). The vanillin measurements also agree

496   quantitatively (slope = 0.92), but the I⁻ CIMS measurement is noisier (R^2= 0.71). For the other three species,

497   the I⁻ CIMS measures only one isomer, while the PTR-ToF measures a sum of several isomers. For all three,

498   the comparison is within the stated uncertainties of both instruments, but the PTR-ToF measurement is

499   lower than the I⁻ CIMS measurement. The PTR-ToF measurement of acrylic acid plus methylglyoxal is

500   31% lower than the I⁻ CIMS measurement of acrylic acid; the PTR-ToF measurement of acetic acid plus

501   glycolaldehyde is 17% lower than the I⁻ CIMS measurement of acetic acid; and the PTR-ToF measurement

502   of cresol plus anisol is 1% lower than the I⁻ CIMS measurement of cresol. The low PTR-ToF measurement

503   for the acrylic acid and cresol comparison is possibly due to uncertainty in the calculated calibration factors,

504   which give the upper limit to sensitivity (and the lower limit to derived concentration). The acetic acid

505   comparison is within the stated uncertainty (27% for PTR-ToF m/z 61.028 $C_2H_4O_2H^+$ and 15% for I⁻ CIMS

506   acetic acid).

507   **3.4 Emission factors, emission ratios, and emission chemistry**

508   We quantified the emission ratios relative to CO, and the emission factors in g/kg fuel burned, of

509   both the identified and unidentified species. The emission ratio (ER) is calculated by Eq. 2:

510    $ER = \frac{\int_{t=0}^{t=end} NMOG - NMOG_{bkgd}\,dt}{\int_{t=0}^{t=end} CO - CO_{bkgd}\,dt}$ Eq. 2

511   where the excess mixing ratios (ppbv above pre-fire chamber background) of the NMOG and of CO are

512   integrated over the fire from time t=0 to t=end. The emission factors (EF) are in units of gram NMOG

513   emitted per kg dry fuel burned, and are derived from the emission ratios using the carbon mass balance

514   (Akagi et al., 2011; Selimovic et al., 2017):

515    $$EF_{NMOG} = F_c \times \frac{M_{NMOG}}{M_C} \times \frac{\left(\Delta NMOG / \Delta CO_2\right)}{\sum_{x=1}^{n}\left(NC_x \times \frac{\Delta C_x}{\Delta CO_2}\right)}$$

516   Where EF_{NMOG} is the emission factor of the NMOG, F_c is the carbon fraction of the fuel in g/kg, M_{NMOG} is

517   the molecular mass of the NMOG, M_C is the molecular mass of carbon, ($\Delta NMOG/\Delta CO_2$) is the emission

518   ratio of the NMOG relative to CO_2 (determined by multiplying the ER by the ratio of CO/CO_2), NC_x is the

519   number of carbon in carbon-containing species x and ($\Delta C_x/\Delta CO_2$) is the emission ratio of species x to CO_2.

520   This method assumes that all of the carbon lost from the fuel as it burns is emitted and measured, which is

Atmospheric
Chemistry
and Physics
Discussions

521   a reasonable approximation as CO, CO_2, and CH_4 account for most of the emitted carbon (Akagi et al.,

522   2011). The denominator of the last term estimates total carbon relative to CO2. Species C_x include all

523   species measured by PTR-ToF, all species measured by FTIR (including CO, CO_2, and CH_4, but excluding

524   overlapped species with PTR-ToF) and black carbon as described by Selimovic et al. (2017). Emission

525   ratios and factors were determined on a fire-by-fire basis, then averaged over all fires (Table 2) or all fires

526   of a particular fuel type (Table S1).

527   The emission ratios and emission factors of the identified compounds averaged over all fires are

528   reported in Table 2. Emission ratios and emission factors of both identified and unidentified compounds

529   for specific fuel types are given in Table S1. The large relative standard deviations of both emission ratio

530   and emission factor, for each NMOG, indicate large differences in emission composition between different

531   fires. Analysis of differences in emissions composition between different fuels and combustion processes

532   will be presented in a separate manuscript. Figure 5 compares the average emission ratios determined in

533   this work to several other studies. Our emission ratios have similar values, ranging from a factor of 1.7

534   higher on average than Gilman et al. (2015) to 0.7 the average of Stockwell et al. (2015). The differences

535   in slopes and scatter are likely due to different fuel types, fire conditions, and sampling strategies. Stockwell

536   et al. (2015) also reported detailed speciation within particular structural categories (non-oxygenated

537   aromatics, phenols, and furans). We compared our speciation for comparable fuel types - coniferous

538   canopy, chaparral, and peat - and the agreement for coniferous fuels and chapparal is within a factor of 2

539   despite differences in ion identification and calibration factor (Fig. 6). The ER to CO are likely the easiest

540   way to incorporate this new NMOG data into models since CO emissions from wildfires are relatively well

541   characterized (Liu et al., 2017b).

542   The 156 PTR ions for which we have identified the NMOG contributors account for a significant

543   fraction of the instrument signal, and total NMOG detected by the PTR-ToF, in each fire. Across all 58

544   stack fires measured with PTR-ToF, an average of 90% of the instrument signal from m/z 12-m/z 217

545   (excluding primary and contaminant ions) is explained by these ions and associated fragments. After

546   calibration, an average of 92% and minimum of 88% of total NMOG mixing ratio detected by PTR-ToF

547   consists of identified compounds (Fig. 7a). The mixing ratios of unidentified species were determined using

548   a calibration factor calculated from the elemental composition of the ion. They are therefore a lower limit

549   and the actual unidentified fraction could be higher (Section 2.3). The PTR-ToF detects about 80-90% of

550   the total NMOG emissions (on a molar basis), based on composition reported by Gilman et al. (2015).

551   In terms of NMOG mass detected by PTR-ToF, an average of 88% and minimum of 82% is

552   accounted for by identified species (Fig 7b). This is an improvement over Warneke et al. (2011), where

553   only 50-75% of the detected mass was identified, and is comparable to Stockwell et al. (2015), with

554   improved identification of emissions from peat, and updated ion assignments (Table S1). Identifying the

Atmospheric
Chemistry
and Physics
Discussions

555   NMOG contributors to additional ions will not increase this by much, because the remaining (unidentified)

556   ions each account for only a small part of the remaining signal. The unidentified portion is a small fraction

557   of the overall detected emissions, but compared to the identified portion, it consists of species that are

558   heavier, contain more oxygen atoms, and are less volatile (Fig. 8). The average molecular mass of

559   unidentified species is 120 u, compared to 50 u for identified species, and species with 3 or more oxygen

560   atoms comprise 24% of unidentified NMOG emissions, but only 2.5% of identified NMOG emissions.

561   Many of the unidentified emissions are of intermediate volatility, while most identified species are highly

562   volatile. Species that could be efficient SOA precursors may therefore be underrepresented in the list of

563   identified NMOGs. Additionally, the heavier, more polar unidentified compounds may be preferentially

564   lost in inlet lines and could comprise a larger fraction of emissions than measured by the PTR-ToF.

565   The detected and identified NMOGs fall into several broad structural categories: furan-type

566   compounds; benzene-type compounds (aromatics); terpenes; non-aromatic molecules containing oxygen,

567   nitrogen, or sulfur; and other hydrocarbons (mostly alkenes). We also included pyrroles, thiophenes, and

568   pyridines as structural categories, but these account for less than 1% of detected emissions on a molar basis.

569   Terpenes include isoprene, monoterpenes, oxygenated monoterpenes, and sesquiterpenes. Non-aromatic

570   oxygen-containing molecules include alkyl carbonyls, esters, and acids. Non-aromatic nitrogen-containing

571   molecules include HCN, HONO, isocyanic acid, methyl isocyanate, amines (including ammonia), and

572   nitriles. Aromatics and furans include alkyl-substituted and oxygenated derivatives of benzene and furan.

573   On average over all fires, non-aromatic oxygenates were the most abundant, comprising 51% of detected

574   emissions (Fig. 9a). The compounds in each category include a range of functional groups, of which

575   alcohols and carbonyls were the most abundant (Fig. 9b). Many compounds also include an alkene

576   functional group. Some compounds, such as guaiacol, have several functional groups. In these cases, the

577   NMOG was counted once in each category.

578   Compared to several previous laboratory studies reporting highly chemically detailed emissions

579   using GC instruments (Hatch et al., 2015;Gilman et al., 2015;Hatch et al., 2017), we observed a similar

580   range and type of speciation for non-oxygenated aromatics, thiophenes, pyrroles, pyridines, alkyl nitriles,

581   alkyl ketones, alkyl esters, and small alcohols. However, this work and a previous PTR-MS study

582   (Stockwell et al., 2015) also observed more highly substituted oxygen-containing aromatics and furans,

583   such as hydroxymethylfuranone and syringol. These substituted compounds contribute significant

584   additional reactivity. For example, Gilman et al. (2015), who studied similar fuels, reported OH reactivity

585   of 1.3-5.5 s^{-1} (ppm CO)$^{-1}$ for furans. In this study, the average OH reactivity of furans is 14.2 s^{-1} (ppm CO)$^{-}$

586   ^{1}. The SOA yields of many of these compounds are unknown but they are likely important SOA precursors

587   (Yee et al., 2013;Gilman et al., 2015;Hatch et al., 2017;Bruns et al., 2016).

Atmospheric
Chemistry
and Physics
Discussions

588   Reaction with the hydroxyl radical (•OH) is an important removal pathway for gas-phase biomass

589   burning emissions in the atmosphere. NMOGs have been previously shown to be an important sink for the

590   OH radical, despite comprising less than 1% by mass of the total measured gas-phase emissions (Gilman

591   et al., 2015). We compiled the rate constants with •OH of the identified species. Where an experimentally

592   determined rate constant was not available, the rate constant of a structurally similar species was used (rate

593   constants and citations in Table S1). On average, furans, aromatics, terpenes, and non-aromatic oxygenates

594   contribute a roughly equal amount to total OH reactivity (Fig. 10a). It has been shown that the average

595   reactivity of NMOG emissions can vary greatly between fuel types (Gilman et al., 2015); here, we show

596   that the average reactivity, and the types of compounds that contribute most to reactivity, also vary greatly

597   over the course of a fire (Fig. 10b). The spike in average reactivity at the beginning of the fire is due to

598   distillation of terpenes.

599   The volatility distribution of emitted species also changes over the course of these lab fires. We

600   determined the saturation vapor concentration (C_0, in $\mu g\ m^{-3}$ at 25ºC) for each of the identified and

601   unidentified species. The values were taken from databases (CRC Handbook, NIST Chemistry WebBook,

602   (Yaws, 2015)) or estimated based on elemental composition via the parameterization described by Li et al.

603   (2016). Species emitted from lower temperature processes during the fire have a higher fraction of

604   compounds with low volatility compared to the high-temperature processes (later and earlier in the fire

605   shown in Fig. 11). Further discussion of chemical differences, and low- and high-temperature processes,

606   will be presented in a separate manuscript (Sekimoto et al., 2017b). The PTR-ToF measures mostly species

607   whose volatility is classified as volatile organic compounds (VOC, $C_0 > 3\times10^6\ \mu g\ m^{-3}$), and a few

608   intermediate volatility compounds (IVOC, $300 < C_0 < 3\times10^6\ \mu g\ m^{-3}$) and semivolatile compounds (SVOC,

609     $0.3 < C_0 < 300\ \mu g\ m^{-3}$) are detected. Many more IVOC species have been measured by 2D-GC (Hatch et

610   al., 2017). It is expected that many species of $C_0 < 10^4\ \mu g\ m^{-3}$ were not transmitted through the transfer inlet

611   and instrument tubing quickly enough to be quantifiable by the PTR-MS (Pagonis et al., 2017).

612   **4. Conclusions**

613   Gas-phase emissions of NMOGs and some inorganic compounds were measured with a high-

614   resolution PTR-ToF instrument during the FIREX 2016 laboratory intensive. Using a combination of

615   techniques, including GC pre-separation, NO^+ CIMS, and time-series correlation, we have identified many

616   more compounds and with greater certainty than has been reported in previous PTR-MS studies of biomass

617   burning emissions. We have identified the NMOG contributors to ~90% of the PTR-ToF signal, accounting

618   for ~90% of the NMOG mass detected by the instrument, and determined the emission factors of these

619   compounds. The NMOG ions not identified are in general larger, more oxygenated, and less volatile than

620 the identified species. This should be considered if using PTR-ToF to study SOA precursors. Unidentified

621 compounds may also be preferentially lost in inlets. The PTR-ToF measurement generally agrees well with

622 other instrumentation for many species. However, small, multiply-oxygenated species such as glyoxal and

623 methylglyoxal may have significant interferences. We determined the reaction rate constant of each

624 identified NMOG with the OH radical. Furans, aromatics, and terpenes are the most important reactive

625 species measured by PTR-ToF. We show that the reactivity of the emissions, volatility of the emissions,

626 and the compounds that contribute to the reactivity can change considerably as different combustion

627 processes occur.

628 This work provides a guide to interpreting PTR-ToF measurements of biomass burning that is

629 strongly supported by literature and complementary analytical techniques. This will serve as a foundation

630 for future use of FIREX 2016 PTR-ToF data, and interpretation of PTR-ToF field measurements. Finally,

631 this work provides the best available emission factors and emission ratios to CO for many wildfire-

632 generated NMOGs.

642 **6. References**

643 Akagi, S. K., Yokelson, R. J., Wiedinmyer, C., Alvarado, M. J., Reid, J. S., Karl, T., Crounse, J. D., and
644 Wennberg, P. O.: Emission factors for open and domestic biomass burning for use in atmospheric models,
645 11, 4039-4072, 10.5194/acp-11-4039-2011, 2011.

646 Alvarado, M. J., Wang, C., and Prinn, R. G.: Formation of ozone and growth of aerosols in young smoke
647 plumes from biomass burning: 2. Three-dimensional Eulerian studies, J. Geophys. Res., 114,
648 10.1029/2008jd011186, 2009.

649 Alvarado, M. J., Lonsdale, C. R., Yokelson, R. J., Akagi, S. K., Coe, H., Craven, J. S., Fischer, E. V.,
650 McMeeking, G. R., Seinfeld, J. H., Soni, T., Taylor, J. W., Weise, D. R., and Wold, C. E.: Investigating the

Atmospheric
Chemistry
and Physics
Discussions

Open Access

651   links between ozone and organic aerosol chemistry in a biomass burning plume from a prescribed fire in
652   California chaparral, Atmos. Chem. Phys., 15, 6667-6688, 10.5194/acp-15-6667-2015, 2015.

653   Breitenlechner, M., Fischer, L., Hainer, M., Heinritzi, M., Curtius, J., and Hansel, A.: PTR3: An Instrument
654   for Studying the Lifecycle of Reactive Organic Carbon in the Atmosphere, Anal. Chem., 89, 5824-5831,
655   10.1021/acs.analchem.6b05110, 2017.

656   Brilli, F., Gioli, B., Ciccioli, P., Zona, D., Loreto, F., Janssens, I. A., and Ceulemans, R.: Proton Transfer
657   Reaction Time-of-Flight Mass Spectrometric (PTR-TOF-MS) determination of volatile organic compounds
658   (VOCs) emitted from a biomass fire developed under stable nocturnal conditions, Atmos. Environ., 97, 54-
659   67, http://dx.doi.org/10.1016/j.atmosenv.2014.08.007, 2014.

660   Bruns, E. A., El Haddad, I., Slowik, J. G., Kilic, D., Klein, F., Baltensperger, U., and Prevot, A. S.:
661   Identification of significant precursor gases of secondary organic aerosols from residential wood
662   combustion, Sci Rep -UK, 6, 27881, doi:10.1038/srep27881, 2016.

663   Bruns, E. A., Slowik, J. G., El Haddad, I., Kilic, D., Klein, F., Dommen, J., Temime-Roussel, B., Marchand,
664   N., Baltensperger, U., and Prévôt, A. S. H.: Characterization of gas-phase organics using proton transfer
665   reaction time-of-flight mass spectrometry: fresh and aged residential wood combustion emissions, Atmos.
666   Chem. Phys., 17, 705-720, 10.5194/acp-17-705-2017, 2017.

667   Burling, I. R., Yokelson, R. J., Griffith, D. W. T., Johnson, T. J., Veres, P., Roberts, J. M., Warneke, C.,
668   Urbanski, S. P., Reardon, J., Weise, D. R., Hao, W. M., and de Gouw, J.: Laboratory measurements of trace
669   gas emissions from biomass burning of fuel types from the southeastern and southwestern United States,
670   Atmos. Chem. Phys., 10, 11115-11130, 10.5194/acp-10-11115-2010, 2010.

671   Christian, T. J.: Comprehensive laboratory measurements of biomass-burning emissions: 1. Emissions from
672   Indonesian, African, and other fuels, J. Geophys. Res., 108, 10.1029/2003jd003704, 2003.

673   Christian, T. J.: Comprehensive laboratory measurements of biomass-burning emissions: 2. First
674   intercomparison of open-path FTIR, PTR-MS, and GC-MS/FID/ECD, J. Geophys. Res., 109,
675   10.1029/2003jd003874, 2004.

676   Collard, F.-X., Blin, J.: A review on pyrolysis of biomass constituents: Mechanisms and composition of the
677   products obtained from the conversion of cellulose, hemiselluloses, and lignin, Renew. Sust. Energ. Rev.,
678   38, 594-608, 10.1016/j.rser.2014.06.013, 2014.

679   Crutzen, P. J., and Andreae, M. O.: Biomass Burning in the Tropics: Impact on Atmospheric Chemistry
680   and Biogeochemical Cycles, Science, 250, 1669-1678, 10.1126/science.250.4988.1669, 1990.

681   de Gouw, J., and Warneke, C.: Measurements of volatile organic compounds in the earth's atmosphere
682   using proton-transfer-reaction mass spectrometry, Mass. Spectrom. Rev., 26, 223-257, 10.1002/mas.20119,
683   2007.

Fu, T.-M., Jacob, D. J., Wittrock, F., Burrows, J. P., Vrekoussis, M., and Henze, D. K.: Global budgets of atmospheric glyoxal and methylglyoxal, and implications for formation of secondary organic aerosols, J. Geophys. Res., 113, 10.1029/2007JD009505, 2008.

Gilman, J. B., Lerner, B. M., Kuster, W. C., Goldan, P. D., Warneke, C., Veres, P. R., Roberts, J. M., de Gouw, J. A., Burling, I. R., and Yokelson, R. J.: Biomass burning emissions and potential air quality impacts of volatile organic compounds and other trace gases from fuels common in the US, Atmos. Chem. Phys., 15, 13915-13938, 10.5194/acp-15-13915-2015, 2015.

Grieshop, A. P., Logue, J. M., Donahue, N. M., and Robinson, A. L.: Laboratory investigation of photochemical oxidation of organic aerosol from wood fires 1: measurement and simulation of organic aerosol evolution, Atmos. Chem. Phys., 9, 1263-1277, 10.5194/acp-9-1263-2009, 2009.

Hatch, L. E., Luo, W., Pankow, J. F., Yokelson, R. J., Stockwell, C. E., and Barsanti, K. C.: Identification and quantification of gaseous organic compounds emitted from biomass burning using two-dimensional gas chromatography–time-of-flight mass spectrometry, Atmos. Chem. Phys., 15, 1865-1899, 10.5194/acp-15-1865-2015, 2015.

Hatch, L. E., Yokelson, R. J., Stockwell, C. E., Veres, P. R., Simpson, I. J., Blake, D. R., Orlando, J. J., and Barsanti, K. C.: Multi-instrument comparison and compilation of non-methane organic gas emissions from biomass burning and implications for smoke-derived secondary organic aerosol precursors, Atmos. Chem. Phys., 17, 1471-1489, 10.5194/acp-17-1471-2017, 2017.

Hays, M. D., Geron, C. D., Linna, K. J., Smith, N. D., and Schauer, J. J.: Speciation of Gas-Phase and Fine Particle Emissions from Burning of Foliar Fuels, Environ. Sci. Technol., 36, 2281-2295, 10.1021/es0111683, 2002.

Heald, C. L., Coe, H., Jimenez, J. L., Weber, R. J., Bahreini, R., Middlebrook, A. M., Russell, L. M., Jolleys, M., Fu, T. M., Allan, J. D., Bower, K. N., Capes, G., Crosier, J., Morgan, W. T., Robinson, N. H., Williams, P. I., Cubison, M. J., DeCarlo, P. F., and Dunlea, E. J.: Exploring the vertical profile of atmospheric organic aerosol: comparing 17 aircraft field campaigns with a global model, Atmos. Chem. Phys., 11, 12673-12696, 10.5194/acp-11-12673-2011, 2011.

Heigenmoser, A., Liebner, F., Windeisen, E., Richter, K.: Investigation of thermally treated beech (*Fagus sylvatica*) and spruce (*Picea abies*) by means of multifunctional analytical pyrolysis-GC/MS, J. Anal. Appl. Pyrol., 100, 117-126, 10.1016/j.jaap.2012.12.005, 2013.

Jaffe, D. A., and Wigder, N. L.: Ozone production from wildfires: A critical review, Atmos. Env., 51, 1-10, 10.1016/j.atmosenv.2011.11.063, 2012.

Jathar, S. H., Gordon, T. D., Hennigan, C. J., Pye, H. O. T., Pouliot, G., Adams, P. J., Donahue, N. M., and Robinson, A. L.: Unspeciated organic emissions from combustion sources and their influence on the secondary organic aerosol budget in the United States, Proc Nat Acad Sci, 111, 10473-10478, 10.1073/pnas.1323740111, 2014.

Atmospheric
Chemistry
and Physics
Discussions

Open Access

719   Jordan, A., Haidacher, S., Hanel, G., Hartungen, E., Märk, L., Seehauser, H., Schottkowsky, R., Sulzer, P.,
720   and Märk, T. D.: A high resolution and high sensitivity proton-transfer-reaction time-of-flight mass
721   spectrometer   (PTR-TOF-MS),   Int.   J.   Mass   Spectrom.,   286,   122-128,
722   http://dx.doi.org/10.1016/j.ijms.2009.07.005, 2009.

723   Karl, T. G., Christian, T. J., Yokelson, R. J., Artaxo, P., Hao, W. M., and Guenther, A.: The Tropical Forest
724   and Fire Emissions Experiment: method evaluation of volatile organic compound emissions measured by
725   PTR-MS, FTIR, and GC from tropical biomass burning, Atmos. Chem. Phys., 7, 5883-5897, 10.5194/acp-
726   7-5883-2007, 2007.

727   Koss, A. R., Warneke, C., Yuan, B., Coggon, M. M., Veres, P. R., and de Gouw, J. A.: Evaluation of NO+
728   reagent ion chemistry for online measurements of atmospheric volatile organic compounds, Atmos. Meas.
729   Tech., 9, 2909-2925, 10.5194/amt-9-2909-2016, 2016.

730   Lee, B. H., Lopez-Hilfiker, F. D., Mohr, C., Kurtén, T., Worsnop, D. R., and Thornton, J. A.: An Iodide-
731   Adduct High-Resolution Time-of-Flight Chemical-Ionization Mass Spectrometer: Application to
732   Atmospheric Inorganic and Organic Compounds, Environ. Sci. Technol., 48, 6309-6317,
733   10.1021/es500362a, 2014.

734   Lerner, B. M., Gilman, J. B., Aikin, K. C., Atlas, E. L., Goldan, P. D., Graus, M., Hendershot, R., Isaacman-
735   VanWertz, G. A., Koss, A., Kuster, W. C., Lueb, R. A., McLaughlin, R. J., Peischl, J., Sueper, D., Ryerson,
736   T. B., Tokarek, T. W., Warneke, C., Yuan, B., and de Gouw, J. A.: An improved, automated whole air
737   sampler and gas chromatography mass spectrometry analysis system for volatile organic compounds in the
738   atmosphere, Atmos. Meas. Tech., 10, 291-313, 10.5194/amt-10-291-2017, 2017.

739   Li, Y., Pöschl, U., and Shiraiwa, M.: Molecular corridors and parameterizations of volatility in the chemical
740   evolution of organic aerosols, Atmos. Chem. Phys., 16, 3327-3344, 10.5194/acp-16-3327-2016, 2016.

741   Liu, W.-J., Li, W.-W., Jiang, H., and Yu, H.-Q.: Fates of Chemical Elements in Biomass during Its
742   Pyrolysis, Chem. Rev., 117, 6367-6398, 10.1021/acs.chemrev.6b00647, 2017a.

743   Liu, X., Huey, L. G., Yokelson, R. J., Selimovic, V., Simpson, I. J., Müller, M., Jimenez, J. L., Campuzano-
744   Jost, P., Beyersdorf, A. J., Blake, D. R., Butterfield, Z., Choi, Y., Crounse, J. D., Day, D. A., Diskin, G. S.,
745   Dubey, M. K., Fortner, E., Hanisco, T. F., Hu, W., King, L. E., Kleinman, L., Meinardi, S., Mikoviny, T.,
746   Onasch, T. B., Palm, B. B., Peischl, J., Pollack, I. B., Ryerson, T. B., Sachse, G. W., Sedlacek, A. J.,
747   Shilling, J. E., Springston, S., St. Clair, J. M., Tanner, D. J., Teng, A. P., Wennberg, P. O., Wisthaler, A.,
748   and G. M. Wolfe.: Airborne measurements of western U.S. wildfire emissions: Comparison with prescribed
749   burning   and   air   quality   implications,   J.   Geophys.   Res.   Atmos.,   122,   6108-6129,
750   doi:10.1002/2016JD026315, 2017b.

751   Lu, Q., Yang, X.-c., Dong, C.-q., Zhang, Z.-f., Zhang, X.-m., and Zhu, X.-f.: Influence of pyrolysis
752   temperature and time on the cellulose fast pyrolysis products: Analytical Py-GC/MS study, J. Anal. Appl.
753   Pyrol., 92, 430-438, http://dx.doi.org/10.1016/j.jaap.2011.08.006, 2011.

754   Min, K. E., Washenfelder, R. A., Dubé, W. P., Langford, A. O., Edwards, P. M., Zarzana, K. J., Stutz, J.,
755   Lu, K., Rohrer, F., Zhang, Y., and Brown, S. S.: A broadband cavity enhanced absorption spectrometer for

Atmospheric
Chemistry
and Physics
Discussions

756   aircraft measurements of glyoxal, methylglyoxal, nitrous acid, nitrogen dioxide, and water vapor, Atmos.
757   Meas. Tech., 9, 423-440, 10.5194/amt-9-423-2016, 2016.

758   Müller, M., Graus, M., Ruuskanen, T. M., Schnitzhofer, R., Bamberger, I., Kaser, L., Titzmann, T.,
759   Hörtnagl, L., Wohlfahrt, G., Karl, T., and Hansel, A.: First eddy covariance flux measurements by PTR-
760   TOF, Atmos. Meas. Tech., 3, 387-395, 10.5194/amt-3-387-2010, 2010.

761   Müller, M., Anderson, B. E., Beyersdorf, A. J., Crawford, J. H., Diskin, G. S., Eichler, P., Fried, A.,
762   Keutsch, F. N., Mikoviny, T., Thornhill, K. L., Walega, J. G., Weinheimer, A. J., Yang, M., Yokelson, R.
763   J., and Wisthaler, A.: In situ measurements and modeling of reactive trace gases in a small biomass burning
764   plume, Atmos. Chem. Phys., 16, 3813-3824, 10.5194/acp-16-3813-2016, 2016.

765   Naeher, L. P., Brauer, M., Lipsett, M., Zelikoff, J. T., Simpson, C. D., Koenig, J. Q., and Smith, K. R.:
766   Woodsmoke Health Effects: A Review, Inhal. Toxicol., 19, 67-106, 10.1080/08958370600985875, 2007.

767   Pagonis, D., Krechmer, J. E., de Gouw, J., Jimenez, J. L., and Ziemann, P. J.: Effects of Gas-Wall
768   Partitioning in Teflon Tubing and Instrumentation on Time-Resolved Measurements of Gas-Phase Organic
769   Compounds, Atmos. Meas. Tech. Discuss., https://doi.org/10.5194/amt-2017-279, in review, 2017.

770   Patwardhan, P. R., Satrio, J. A., Brown, R. C., and Shanks, B. H.: Product distribution from fast pyrolysis
771   of   glucose-based   carbohydrates,   J.   Anal.   Appl.   Pyrol.,   86,   323-330,
772   https://doi.org/10.1016/j.jaap.2009.08.007, 2009.

773   Reddington, C. L., Spracklen, D. V., Artaxo, P., Ridley, D. A., Rizzo, L. V., and Arana, A.: Analysis of
774   particulate emissions from tropical biomass burning using a global aerosol model and long-term surface
775   observations, Atmos. Chem. Phys., 16, 11083-11106, 10.5194/acp-16-11083-2016, 2016.

776   Roberts, J. M., Veres, P., Warneke, C., Neuman, J. A., Washenfelder, R. A., Brown, S. S., Baasandorj, M.,
777   Burkholder, J. B., Burling, I. R., Johnson, T. J., Yokelson, R. J., and de Gouw, J.: Measurement of HONO,
778   HNCO, and other inorganic acids by negative-ion proton-transfer chemical-ionization mass spectrometry
779   (NI-PT-CIMS): Application to biomass burning emissions., Atmos. Meas. Tech., 3, 981-990, 2010.

780   Sekimoto, K., Li, S.-M., Yuan, B., Koss, A., Coggon, M. M., Warnke, C., and de Gouw, J.: Calculation of
781   the sensitivity of proton-transfer-reaction mass spectrometry (PTR-MS) for organic trace gases, Int. J. Mass
782   Spectrom., in press, 10.1016/j.ijms.2017.04.006, 2017a.

783   Sekimoto, K., Koss, A., Yuan, B., Coggon, M. M., Selimovic, V., Warneke, C., Yokelson, R., and De
784   Gouw, J.: High- and low-temperature pytolysis profiles predict primary emissions of volatile organic
785   compounds from biomass burning of fuels common in the western US, in preparation, 2017b.

786   Selimovic, V., Yokelson, R. J., Warneke, C., Roberts, J. M., de Gouw, J., Reardon, J., and Griffith, D. W.
787   T.: Aerosol optical properties and trace gas emissions by PAX and OP-FTIR for laboratory-simulated
788   western US wildfires during FIREX, submitted, Atmos. Chem. Phys., acp-2017-859, 2017.

789   Shrivastava, M., Cappa, C. D., Fan, J., Goldstein, A. H., Guenther, A. B., Jimenez, J. L., Kuang, C., Laskin,
790   A., Martin, S. T., Ng, N. L., Petaja, T., Pierce, J. R., Rasch, P. J., Roldin, P., Seinfeld, J. H., Shilling, J.,

Smith, J. N., Thornton, J. A., Volkamer, R., Wang, J., Worsnop, D. R., Zaveri, R. A., Zelenyuk, A. and Zhang, Q.: Recent advances in understanding secondary organic aerosol: Implications for global climate forcing, Rev. Geophys., 55(2), 509–559, doi:10.1002/2016RG000540, 2017.

Stockwell, C. E., Yokelson, R. J., Kreidenweis, S. M., Robinson, A. L., DeMott, P. J., Sullivan, R. C., Reardon, J., Ryan, K. C., Griffith, D. W. T., and Stevens, L.: Trace gas emissions from combustion of peat, crop residue, domestic biofuels, grasses, and other fuels: configuration and Fourier transform infrared (FTIR) component of the fourth Fire Lab at Missoula Experiment (FLAME-4), Atmos. Chem. Phys., 14, 9727-9754, 10.5194/acp-14-9727-2014, 2014.

Stockwell, C. E., Veres, P. R., Williams, J., and Yokelson, R. J.: Characterization of biomass burning emissions from cooking fires, peat, crop residue, and other fuels with high-resolution proton-transfer-reaction time-of-flight mass spectrometry, Atmos. Chem. Phys., 15, 845-865, 10.5194/acp-15-845-2015, 2015.

Stockwell et al., Laboratory characterization and calibration of aerosols using a total reactive nitrogen system (N_r) and evaluation of an on-line particle-into-liquid sampler coupled with an electrospray ionization source (PiLS-ESI/MS), in preparation for submission to Atmos. Meas. Technol., 2017.

Stönner, C., Derstroff, B., Klüpfel, T., Crowley, J. N., and Williams, J.: Glyoxal measurement with a proton transfer reaction time of flight mass spectrometer (PTR-TOF-MS): characterization and calibration, J. Mass Spectrom., 52, 30-35, 10.1002/jms.3893, 2017.

Veres, P., Gilman, J. B., Roberts, J. M., Kuster, W. C., Warneke, C., Burling, I. R., and de Gouw, J.: Development and validation of a portable gas phase standard generation and calibration system for volatile organic compounds, Atmos. Meas. Tech., 3, 683-691, 10.5194/amt-3-683-2010, 2010a.

Veres, P., Roberts, J. M., Burling, I. R., Warneke, C., de Gouw, J., and Yokelson, R. J.: Measurements of gas-phase inorganic and organic acids from biomass fires by negative-ion proton-transfer chemical-ionization mass spectrometry, J. Geophys. Res., 115, 10.1029/2010jd014033, 2010b.

Warneke, C., de Gouw, J. A., Kuster, W. C., Goldan, P. D., and Fall, R.: Validation of Atmospheric VOC Measurements by Proton-Transfer- Reaction Mass Spectrometry Using a Gas-Chromatographic Preseparation Method, Environ. Sci. Technol., 37, 2494-2501, 10.1021/es026266i, 2003.

Warneke, C., Roberts, J. M., Veres, P., Gilman, J., Kuster, W. C., Burling, I., Yokelson, R., and de Gouw, J. A.: VOC identification and inter-comparison from laboratory biomass burning using PTR-MS and PIT-MS, Int. J. Mass Spectrom., 303, 6-14, 10.1016/j.ijms.2010.12.002, 2011.

Wiedinmyer, C., Akagi, S. K., Yokelson, R. J., Emmons, L. K., Al-Saadi, J. A., Orlando, J. J., and Soja, A. J.: The Fire INventory from NCAR (FINN): a high resolution global model to estimate the emissions from open burning, Geosci. Model Dev., 4, 625-641, 10.5194/gmd-4-625-2011, 2011.

Yaws, C. L.: The Yaws Handbook of Vapor Pressure: Antoine Coefficients, Elsevier Science, 2015.

Atmospheric
Chemistry
and Physics
Discussions

825 Yee, L. D., Kautzman, K. E., Loza, C. L., Schilling, K. A., Coggon, M. M., Chhabra, P. S., Chan, M. N.,
826 Chan, A. W. H., Hersey, S. P., Crounse, J. D., Wennberg, P. O., Flagan, R. C., and Seinfeld, J. H.: Secondary
827 organic aerosol formation from biomass burning intermediates: phenol and methoxyphenols, Atmos. Chem.
828 Phys., 13, 8019-8043, 10.5194/acp-13-8019-2013, 2013.

829 Yokelson, R. J., Griffith, D. W. T., and Ward, D. E.: Open-path Fourier transform infrared studies of large-
830 scale laboratory biomass fires, J. Geophys. Res., 101, 21067, 10.1029/96jd01800, 1996.

831 Yokelson, R. J., Crounse, J. D., DeCarlo, P. F., Karl, T., Urbanski, S., Atlas, E., Campos, T., Shinozuka,
832 Y., Kapustin, V., Clarke, A. D., Weinheimer, A., Knapp, D. J., Montzka, D. D., Holloway, J., Weibring,
833 P., Flocke, F., Zheng, W., Toohey, D., Wennberg, P. O., Wiedinmyer, C., Mauldin, L., Fried, A., Richter,
834 D., Walega, J., Jimenez, J. L., Adachi, K., Buseck, P. R., Hall, S. R., and Shetter, R.: Emissions from
835 biomass burning in the Yucatan, Atmos. Chem. Phys., 9, 5785-5812, 10.5194/acp-9-5785-2009, 2009.

836 Yokelson, R. J., Burling, I. R., Gilman, J. B., Warneke, C., Stockwell, C. E., de Gouw, J., Akagi, S. K.,
837 Urbanski, S. P., Veres, P., Roberts, J. M., Kuster, W. C., Reardon, J., Griffith, D. W. T., Johnson, T. J.,
838 Hosseini, S., Miller, J. W., Cocker Iii, D. R., Jung, H., and Weise, D. R.: Coupling field and laboratory
839 measurements to estimate the emission factors of identified and unidentified trace gases for prescribed fires,
840 Atmos. Chem. Phys., 13, 89-116, 10.5194/acp-13-89-2013, 2013.

841 Yuan, B., Warneke, C., Shao, M., and de Gouw, J. A.: Interpretation of volatile organic compound
842 measurements by proton-transfer-reaction mass spectrometry over the deepwater horizon oil spill, Int. J.
843 Mass Spectrom., 358, 43-48, http://dx.doi.org/10.1016/j.ijms.2013.11.006, 2014.

844 Yuan, B., Koss, A., Warneke, C., Gilman, J. B., Lerner, B. M., Stark, H., and de Gouw, J. A.: A high-
845 resolution time-of-flight chemical ionization mass spectrometer utilizing hydronium ions (H3O+ ToF-
846 CIMS) for measurements of volatile organic compounds in the atmosphere, Atmos. Meas. Tech., 9, 2735-
847 2752, 10.5194/amt-9-2735-2016, 2016.

848 Yuan, B., Koss, A. R., Warneke, C., Coggon, M., Sekimoto, K. and de Gouw, J. A.: Proton-Transfer-
849 Reaction Mass Spectrometry: Applications in Atmospheric Sciences, Chem. Rev., acs.chemrev.7b00325,
850 doi:10.1021/acs.chemrev.7b00325, 2017.

851 Zhang, X., Yang, W., and Blasiak, W.: Thermal decomposition mechanism of levoglucosan during
852 cellulose pyrolysis, 96, 110-119, http://dx.doi.org/10.1016/j.jaap.2012.03.012, 2012.

Atmospheric
Chemistry
and Physics
Discussions

Table 1

Instrumentation details.

Instrument	Operating principle	Species measured	Time resolution	Detection limits	Inlet setup	Reference
PTR-ToF	Chemical ionization mass spectrometry; H_3O^+ reagent ions	Polar and unsaturated NMOG (several hundred)	2 Hz	20 pptv (acrylonitrile) to 2.6 ppb (H_2S) at 1Hz resolution	Stack: from sampling platform, 16m long. Room: from 3m above combustion chamber floor, 7m long. Both: ½" OD PFA inlet, 40°C, flow rate 100 lpm. Subsample 500 sccm through PEEK capillary.	Yuan et al. (2016)
NO^+-CIMS	Chemical ionization mass spectrometry; NO^+ reagent ions	Saturated, unsaturated, and polar NMOG (several hundred)	2 Hz	20 pptv (aromatics) to 19 ppb (methanol) at 1Hz resolution	Same as PTR-ToF.	Koss et al., (2016)
GC-EI-MS	Gas chromatographic (GC) separation with electron-ionization quadrupole mass spectrometry (EI-MS)	NMOG (several hundred)	4 minute sample (240 sccm) every 20 minutes	<5 pptv (most species) for 4-minute sample	Stack: from sampling platform, 16m long, ½" OD PFA inlet, flow rate 20 lpm. Room: from 3m above combustion chamber floor, 7m long, ¼" OD PFA, flow rate 2-7 lpm. Both: Dynamically diluted with UHP N_2.	Lerner et al. (2017)
GC-CIMS	Gas chromatographic separation with chemical ionization mass spectrometry (CIMS)	Polar and unsaturated NMOG (several hundred)	4 minute sample every 20 minutes	qualitative measurement only	Same as GC-EI-MS	
OP-FTIR	Open path FTIR absorption spectroscopy	Small organic and inorganic trace gases (about 20)	0.73 Hz	1 ppbv at 0.73 Hz resolution	From sampling platform (no inlet).	Stockwell et al. (2014)
ACES	Broadband cavity enhanced spectroscopy ("Airborne Cavity Enhanced Spectrometer")	Glyoxal, NO_2, HONO, methyl glyoxal	1 Hz	100 pptv (glyoxal) to 2 ppbv (HONO); ~5 ppbv for methylgyloxal	Stack: from sampling platform, 1m long ¼" OD PFA including particle filter	Min et al. (2016)
I^- CIMS	Chemical ionization mass spectrometry; I^- reagent ions	Polar NMOG (several hundred)	1 Hz	1 pptv (malonic acid) to 1.5 ppbv (peroxyacetic acid)	Shared with PTR-ToF. Stack: from sampling platform, 16m long.	Lee et al. (2014)

Atmospheric
Chemistry
and Physics
Discussions

Open Access

EGU

| | | | | at 1Hz resolution | Room: from 3m above combustion chamber floor, 7m long. Both: ½" OD PFA inlet, flow rate 100 lpm. | |

Table 2

Ion exact masses, formulas, and NMOG contributor(s); and the emission ratios and emission factors of those contributors.

Ion exact m/z (Th)	Ion Formula	NMOG contributor(s) (details in Table S1)	ER to CO, ppb/ppm (σ)	EF, g/kg (σ)
18.034	NH_3H^+	ammonia	17 (13)	0.82 (0.80)
26.015	$C_2H_2^+$	acetylene	5.0 (2.5)	0.36 (0.24)
28.018	$HCNH^+$	Hydrogen cyanide	3.9 (3.6)	0.33 (0.47)
28.031	$C_2H_4^+$	ethene	7.1 (3.8)	0.54 (0.38)
30.034	CH_3NH^+	Methanimine	0.0092 (0.012)	0.00073 (0.0010)
31.018	CH_2OH^+	Formaldehyde	20 (10)	1.7 (1.2)
33.034	CH_4OH^+	Methanol	12 (5.9)	1.1 (0.82)
34.995	H_2SH^+	Hydrogen sulfide	0.26 (0.51)	0.029 (0.062)
42.034	$C_2H_3NH^+$	Acetonitrile	1.0 (1.4)	0.13 (0.22)
43.054	$C_3H_6H^+$	Propene	4.5 (2.9)	0.55 (0.44)
44.013	$HNCOH^+$	Isocyanic acid	4.6 (2.5)	0.53 (0.34)
44.050	$C_2H_5NH^+$	Etheneamine	0.052 (0.055)	0.0064 (0.0069)
45.034	$C_2H_4OH^+$	Acetaldehyde	7.4 (5.2)	0.92 (0.73)
46.029	CH_3NOH^+	Formamide	0.10 (0.12)	0.013 (0.018)
46.065	$C_2H_7NH^+$	Ethylamine	0.0030 (0.0080)	0.00038 (0.0010)
47.013	$CH_2O_2H^+$	Formic acid	2.2 (1.4)	0.28 (0.22)
47.049	$C_2H_6OH^+$	ethanol	0.56 (0.92)	0.072 (0.11)
48.008	HNO_2H^+	Nitrous acid	4.1 (1.8)	0.49 (0.23)
49.011	CH_4SH^+	methane thiol	0.13 (0.27)	0.020 (0.043)
49.028	$CH_4O_2H^+$	Methanediol	0.0040 (0.0028)	0.00051 (0.00039)
52.018	C_3HNH^+	Propyne nitrile	0.0090 (0.0068)	0.0013 (0.0011)
53.039	$C_4H_4H^+$	1-Buten-3-yne	0.35 (0.20)	0.049 (0.035)
54.034	$C_3H_3NH^+$	acrylonitrile	0.16 (0.12)	0.025 (0.021)
55.018	$C_3H_2OH^+$	2-propynal	0.20 (0.10)	0.029 (0.019)
55.054	$C_4H_6H^+$	Butadienes	1.8 (1.2)	0.28 (0.23)
56.050	$C_3H_5NH^+$	Propanenitrile	0.10 (0.14)	0.017 (0.027)
57.034	$C_3H_4OH^+$	Acrolein	5.4 (3.0)	0.80 (0.52)
57.070	$C_4H_8H^+$	Butenes, other hydrocarbon	1.2 (1.0)	0.21 (0.21)
58.029	$C_2H_3NOH^+$	methyl isocyanate, hydroxy acetonitrile	0.089 (0.086)	0.015 (0.016)
58.065	$C_3H_7NH^+$	Propene amine	0.022 (0.034)	0.0036 (0.0059)
59.013	$C_2H_2O_2H^+$	glyoxal	1.7 (1.3)	0.26 (0.23)
59.049	$C_3H_6OH^+$	Acetone	2.3 (1.7)	0.39 (0.35)
60.044	$C_2H_5NOH^+$	acetamide	0.46 (1.1)	0.086 (0.21)
60.081	$C_3H_9NH^+$	C3 amines	0.023 (0.052)	0.0041 (0.010)
61.028	$C_2H_4O_2H^+$	acetic acid, glycolaldehyde	15 (11)	2.5 (2.2)
62.024	$CH_3NO_2H^+$	nitromethane	0.34 (0.21)	0.053 (0.036)
63.026	$C_2H_6SH^+$	Dimethyl sulfide	0.012 (0.018)	0.0024 (0.0041)
66.034	$C_4H_3NH^+$	butynenitriles, cyanoallene	0.0020 (0.0017)	0.00037 (0.00035)
67.054	$C_5H_6H^+$	1,3-cyclopentadiene	0.16 (0.13)	0.030 (0.029)
68.050	$C_4H_5NH^+$	butenenitrile isomers, pyrrole	0.36 (0.46)	0.071 (0.10)
68.997	$C_3O_2H^+$	carbon suboxide	0.016 (0.0093)	0.0028 (0.0018)
69.034	$C_4H_4OH^+$	furan	1.9 (1.1)	0.36 (0.25)
69.070	$C_5H_8H^+$	Isoprene	1.0 (0.82)	0.21 (0.20)
70.065	$C_4H_7NH^+$	Butanenitriles, dihydropyrrole	0.076 (0.12)	0.016 (0.028)

| 71.013	$C_3H_2O_2H^+$	Propiolic acid	0.046 (0.025)	0.0088 (0.0057)
71.049	$C_4H_6OH^+$	MVK, methacrolein, crotonaldehyde	1.7 (1.0)	0.32 (0.21)
71.086	$C_5H_{10}H^+$	Pentenes, methylbutenes	0.12 (0.11)	0.026 (0.029)
72.081	$C_4H_9NH^+$	butene amines, tetrahydropyrrole	0.0077 (0.014)	0.0016 (0.0031)
73.028	$C_3H_4O_2H^+$	methyl glyoxal, acrylic acid	1.4 (1.0)	0.28 (0.19)
73.065	$C_4H_8OH^+$	MEK, 2-methylpropanal, butanal	0.52 (0.50)	0.11 (0.13)
74.024	$C_2H_3NO_2H^+$	nitroethene	0.0068 (0.0039)	0.0013 (0.00084)
75.044	$C_3H_6O_2H^+$	hydroxyacetone, methyl acetate, ethyl formate	2.8 (2.3)	0.55 (0.45)
76.039	$C_2H_5NO_2H^+$	nitroethane	0.0034 (0.0022)	0.00072 (0.00057)
78.001	CH_3NOSH^+	n-sulfinylmethanamine	0.00031 (0.00022)	6.9e-05 (5.9e-05)
79.054	$C_6H_6H^+$	benzene	1.7 (1.1)	0.37 (0.30)
80.050	$C_5H_5NH^+$	pyridine, C5 nitriles	0.13 (0.18)	0.031 (0.049)
81.034	$C_5H_4OH^+$	2,4-Cyclopentadiene-1-one, other hydrocarbon	0.61 (0.40)	0.13 (0.093)
82.065	$C_5H_7NH^+$	methylpyrrole, pentenenitriles	0.093 (0.15)	0.023 (0.041)
83.049	$C_5H_6OH^+$	methylfurans, other hydrocarbon	1.51 (1.01)	0.35 (0.28)
84.081	$C_5H_9NH^+$	Pentanenitriles	0.035 (0.066)	0.0094 (0.019)
85.011	$C_4H_4SH^+$	thiophene	0.057 (0.041)	0.014 (0.011)
85.028	$C_4H_4O_2H^+$	2-(3H)-furanone	1.7 (1.1)	0.39 (0.30)
85.065	$C_5H_8OH^+$	3-methyl-3-butene-2-one, cyclopentanone, other hydrocarbon	0.52 (0.35)	0.12 (0.10)
87.044	$C_4H_6O_2H^+$	2,3-butanedione, methyl acrylate, other hydrocarbon	2.0 (1.7)	0.46 (0.35)
87.080	$C_5H_{10}OH^+$	3-methyl-2-butanone, methylbutanals, pentanones	0.16 (0.20)	0.042 (0.059)
89.023	$C_3H_4O_3H^+$	pyruvic acid	0.041 (0.027)	0.010 (0.0070)
89.060	$C_4H_8O_2H^+$	Methyl propanoate	0.34 (0.27)	0.081 (0.067)
90.055	$C_3H_7NO_2H^+$	nitropropanes	0.0022 (0.0037)	0.00056 (0.0010)
92.050	$C_6H_6N^+$	ethynylpyrrole	0.0066 (0.0054)	0.0017 (0.0016)
93.070	$C_7H_8H^+$	toluene	0.9 (0.72)	0.24 (0.24)
94.029	C_5H3NOH^+	Furan carbonitriles	0.01 (0.012)	0.0031 (0.0044)
94.065	$C_6H_7NH^+$	methylpyridines	0.075 (0.12)	0.022 (0.037)
94.998	$C_2H_6S_2H^+$	dimethyl disulfide	0.0082 (0.0064)	0.0022 (0.0020)
95.049	$C_6H_6OH^+$	phenol	2.0 (1.4)	0.55 (0.46)
96.044	$C_5H_5NOH^+$	4-Pyridinol	0.048 (0.071)	0.014 (0.021)
96.081	$C_6H_9NH^+$	C2-substituted pyrroles	0.043 (0.081)	0.013 (0.025)
97.028	$C_5H_4O_2H^+$	Furfurals, other hydrocarbons	2.1 (1.4)	0.60 (0.58)
97.065	$C_6H_8OH^+$	C2-substituted furans	0.83 (0.65)	0.22 (0.20)
98.096	$C_6H_{11}NH^+$	4-methylpentanenitrile	0.013 (0.026)	0.004 (0.0084)
99.026	$C_5H_6SH^+$	methylthiophene	0.079 (0.072)	0.021 (0.020)
99.044	$C_5H_6O_2H^+$	2-methanol furanone	1.5 (1.1)	0.40 (0.31)
99.080	$C_6H_{10}OH^+$	Methylcyclopentanone, cyclohexanone, hexenones	0.086 (0.087)	0.024 (0.028)
101.023	$C_4H_4O_3H^+$	Dihydrofurandione	0.18 (0.15)	0.052 (0.052)
101.060	$C_5H_8O_2H^+$	methyl methacrylate, other hydrocarbon	0.51 (0.34)	0.14 (0.10)
101.096	$C_6H_{12}OH^+$	hexanals, hexanones	0.017 (0.021)	0.0052 (0.0072)
103.039	$C_4H_6O_3H^+$	acetic anhydride,	0.34 (0.28)	0.092 (0.075)
103.054	$C_8H_6H^+$	Phenylacetylene	0.039 (0.037)	0.011 (0.012)
104.049	$C_7H_5NH^+$	Benzonitrile	0.076 (0.057)	0.023 (0.024)
105.070	$C_8H_8H^+$	styrene	0.27 (0.21)	0.079 (0.073)
106.065	$C_7H_7NH^+$	vinyl pyridine	0.010 (0.011)	0.0033 (0.0038)
107.049	$C_7H_6OH^+$	benzaldehyde	0.26 (0.15)	0.079 (0.056)

107.086	$C_8H_{10}H^+$	C8 aromatics	0.40 (0.33)	0.13 (0.13)
108.044	$C_6H_5NOH^+$	pyridine aldehyde	0.018 (0.015)	0.0058 (0.0059)
108.081	$C_7H_9NH^+$	dimethyl + ethyl pyridine, heptyl nitriles	0.027 (0.052)	0.009 (0.018)
109.028	$C_6H_4O_2H^+$	Quinone	0.34 (0.27)	0.093 (0.065)
109.065	$C_7H_8OH^+$	Cresol, anisole	1.5 (1.0)	0.46 (0.39)
110.096	$C_7H_{11}NH^+$	C7 acrylonitriles, C3-substituted pyrroles	0.017 (0.032)	0.0057 (0.012)
111.044	$C_6H_6O_2H^+$	methyl furfural, benzene diols, 2-acetyl furan	2.4 (1.4)	0.75 (0.62)
111.080	$C_7H_{10}OH^+$	C3-substituted furans, other compounds	0.3 (0.27)	0.093 (0.10)
112.039	$C_5H_5NO_2H^+$	dihydroxy pyridine, methyl maleimide	0.021 (0.023)	0.0071 (0.0088)
113.023	$C_5H_4O_3H^+$	5-Hydroxy 2-furfural, 2-furoic acid	0.32 (0.22)	0.11 (0.10)
113.060	$C_6H_8O_2H^+$	2-hydroxy-3-methyl-2-cyclopenten-1-one	0.67 (0.50)	0.21 (0.17)
113.096	$C_7H_{12}OH^+$	ethyl cyclopentanone	0.036 (0.034)	0.012 (0.013)
114.019	$C_4H_3NO_3H^+$	nitrofuran	0.0037 (0.0025)	0.0012 (0.001)
115.039	$C_5H_6O_3H^+$	5-hydroxymethyl-2[3H]-furanone	0.63 (0.52)	0.20 (0.18)
115.075	$C_6H_{10}O_2H^+$	C6 diketone isomers, C6 esters	0.10 (0.074)	0.032 (0.028)
115.112	$C_7H_{14}OH^+$	Heptanal, 2,4-dimethyl-3-pentanone, heptanone	0.030 (0.030)	0.010 (0.011)
117.055	$C_5H_8O_3H^+$	2,5-Dihydroxymethyl dihydrofurfural	0.43 (0.50)	0.13 (0.12)
117.070	$C_9H_8H^+$	Indene, methyl ethynyl benzene	0.081 (0.081)	0.027 (0.031)
117.091	$C_6H_{12}O_2H^+$	butyl ester acetic acid, other C6 esters	0.033 (0.045)	0.012 (0.019)
118.050	$C_4H_7NO_3H^+$	butene nitrates	0.008 (0.0066)	0.0027 (0.0025)
118.065	$C_8H_7NH^+$	Benzeneacetonitrile	0.032 (0.039)	0.011 (0.015)
119.049	$C_8H_6OH^+$	benzofuran	0.12 (0.088)	0.038 (0.029)
119.086	$C_9H_{10}H^+$	MethylStyrene, propenyl benzene+methyl ethenyl benzene, indane	0.12 (0.10)	0.043 (0.043)
120.081	$C_8H_9NH^+$	dihydro pyridine	0.0049 (0.0075)	0.0018 (0.0029)
121.065	$C_8H_8OH^+$	Tolualdehyde	0.34 (0.31)	0.11 (0.11)
121.101	$C_9H_{12}H^+$	C9 aromatics	0.15 (0.13)	0.056 (0.060)
123.044	$C_7H_6O_2H^+$	Salicyladehyde	0.21 (0.15)	0.074 (0.070)
123.080	$C_8H_{10}OH^+$	ethylphenol+dimethylphenol, methylanisole	0.37 (0.28)	0.13 (0.12)
124.039	$C_6H_5NO_2H^+$	nitrobenzene	0.019 (0.013)	0.0068 (0.0062)
125.023	$C_6H_4O_3H^+$	hydroxy benzoquinone	0.18 (0.10)	0.060 (0.044)
125.060	$C_7H_8O_2H^+$	guaiacol	1.3 (1.0)	0.48 (0.59)
126.128	$C_8H_{15}NH^+$	C8 nitriles	0.0015 (0.0042)	0.00062 (0.0017)
126.970	$C_2H_6S_3H^+$	dimethyl trisulfide	0.0024 (0.0036)	0.00081 (0.0011)
127.039	$C_6H_6O_3H^+$	5-hydroxymethyl 2-furfural	0.88 (0.65)	0.32 (0.32)
129.055	$C_6H_8O_3H^+$	2,5-di(hydroxymethyl)furan, methyl hydroxy dihydrofurfural	0.39 (0.27)	0.14 (0.13)
129.070	$C_{10}H_8H^+$	Naphthalene	0.20 (0.16)	0.07 (0.067)
131.086	$C_{10}H_{10}H^+$	Dihydronaphthalene	0.078 (0.063)	0.030 (0.030)
132.081	$C_9H_9NH^+$	MethylBenzeneAcetonitrile	0.014 (0.020)	0.0056 (0.0088)
133.065	$C_9H_8OH^+$	Methylbenzofurans	0.19 (0.35)	0.068 (0.11)
133.101	$C_{10}H_{12}H^+$	EthylStyrene, butenyl benzene isomers, MethylIndane	0.086 (0.071)	0.034 (0.033)
135.080	$C_9H_{10}OH^+$	methyl acetophenone	0.11 (0.073)	0.041 (0.033)
135.117	$C_{10}H_{14}H^+$	C10 aromatics	0.11 (0.10)	0.045 (0.049)
137.060	$C_8H_8O_2H^+$	Methylbenzoicacid	0.22 (0.13)	0.083 (0.063)
137.132	$C_{10}H_{16}H^+$	monoterpenes	2.7 (4.2)	1.1 (2.0)
138.055	$C_7H_7NO_2H^+$	nitrotoluene	0.019 (0.023)	0.0080 (0.011)
139.075	$C_8H_{10}O_2H^+$	methylguaicol	0.77 (0.63)	0.34 (0.46)
143.086	$C_{11}H_{10}H^+$	Methyl naphthalene	0.08 (0.063)	0.033 (0.032)
145.050	$C_6H_8O_4H^+$	Levoglucosan pyrolysis product	0.35 (0.27)	0.15 (0.17)
145.065	$C_{10}H_8OH^+$	2-ethenyl benzofuran	0.05 (0.037)	0.020 (0.018)

Atmospheric
Chemistry
and Physics
Discussions

145.101	$C_{11}H_{12}H^+$	ethylindene	0.037 (0.036)	0.016 (0.019)
147.080	$C_{10}H_{10}OH^+$	dimethylbenzofuran, ethyl benzofuran	0.10 (0.065)	0.043 (0.034)
149.096	$C_{10}H_{12}OH^+$	estragole	0.069 (0.066)	0.029 (0.033)
149.132	$C_{11}H_{16}H^+$	C11 aromatics	0.026 (0.022)	0.012 (0.012)
151.075	$C_9H_{10}O_2H^+$	vinylguaiacol	0.35 (0.31)	0.15 (0.16)
153.055	$C_8H_8O_3H^+$	Vanillin	0.37 (0.31)	0.17 (0.22)
153.070	$C_{12}H_8H^+$	acenaphthylene	0.025 (0.026)	0.010 (0.013)
153.127	$C_{10}H_{16}OH^+$	Camphor, other oxygenated monoterpenes	0.070 (0.15)	0.031 (0.066)
155.070	$C_8H_{10}O_3H^+$	syringol	0.12 (0.14)	0.046 (0.055)
155.143	$C_{10}H_{18}OH^+$	Cineole, other oxygenated monoterpenes	0.013 (0.012)	0.0059 (0.0061)
157.101	$C_{12}H_{12}H^+$	C2-substituted naphthalenes	0.051 (0.039)	0.024 (0.025)
157.159	$C_{10}H_{20}OH^+$	Decanal	0.0051 (0.0051)	0.0024 (0.0030)
163.148	$C_{12}H_{18}H^+$	C12 aromatics	0.013 (0.012)	0.0067 (0.0073)
165.091	$C_{10}H_{12}O_2H^+$	Eugenol, isoeugenol	0.22 (0.17)	0.11 (0.12)
177.164	$C_{13}H_{20}H^+$	C13 aromatics	0.0094 (0.0079)	0.0053 (0.0058)
205.195	$C_{15}H_{24}H^+$	Sesquiterpenes	0.15 (0.13)	0.090 (0.090)

Figure 1
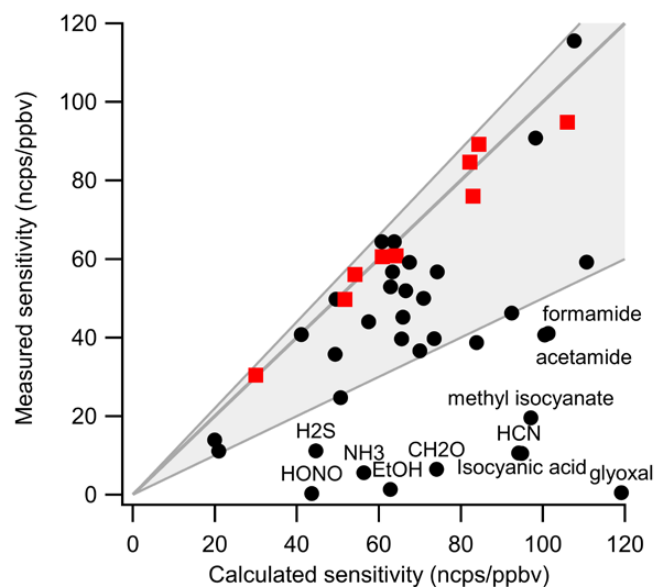
Comparison of measured and calculated calibration factors for several NMOGs. The nine compounds used to determine the calibration proportionality constant are highlighted as red squares. The shaded area shows an uncertainty of +10%/-50%. HONO, HCN, and ammonia sensitivities were derived from comparison with FTIR and are included as "measured" sensitivities.

Figure 2
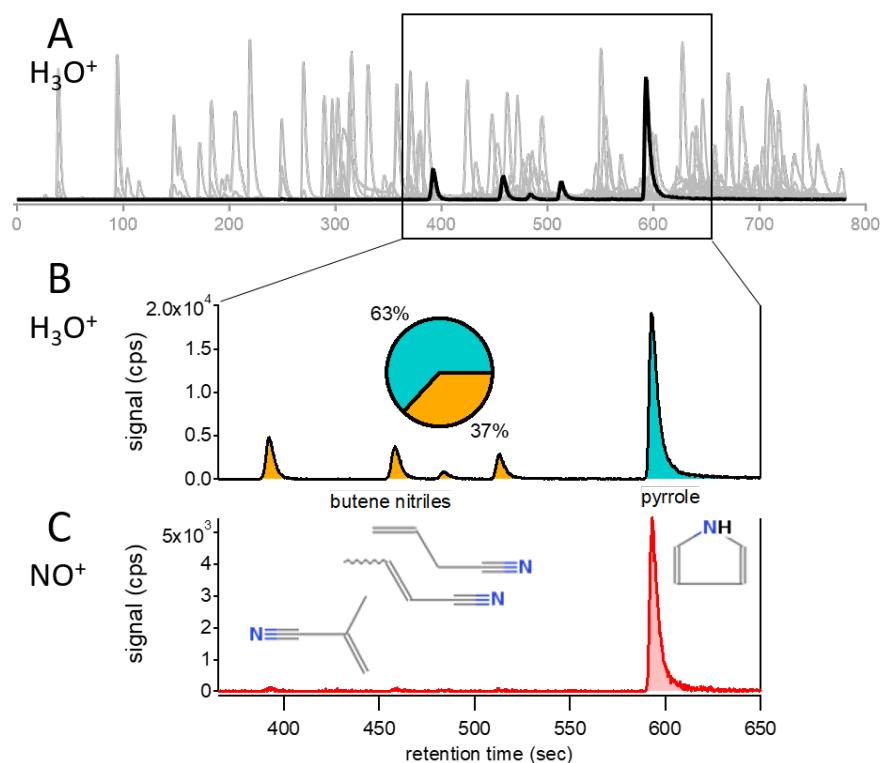
(A) GC-PTR-ToF chromatograph of emissions from a Douglas fir fire. (B) Several chromatographic peaks containing m/z 68.050 $C_4H_5NH^+$ detected during the highlighted elution period in (A). The inset pie chart shows the relative contributions of the isomers to total signal of $C_4H_5NH^+$. (C) GC-NO$^+$-C chromatographic trace of m/z 67.042 $C_4H_5N^+$ from the same Douglas fir fire. Only pyrrole is observed.

Figure 3
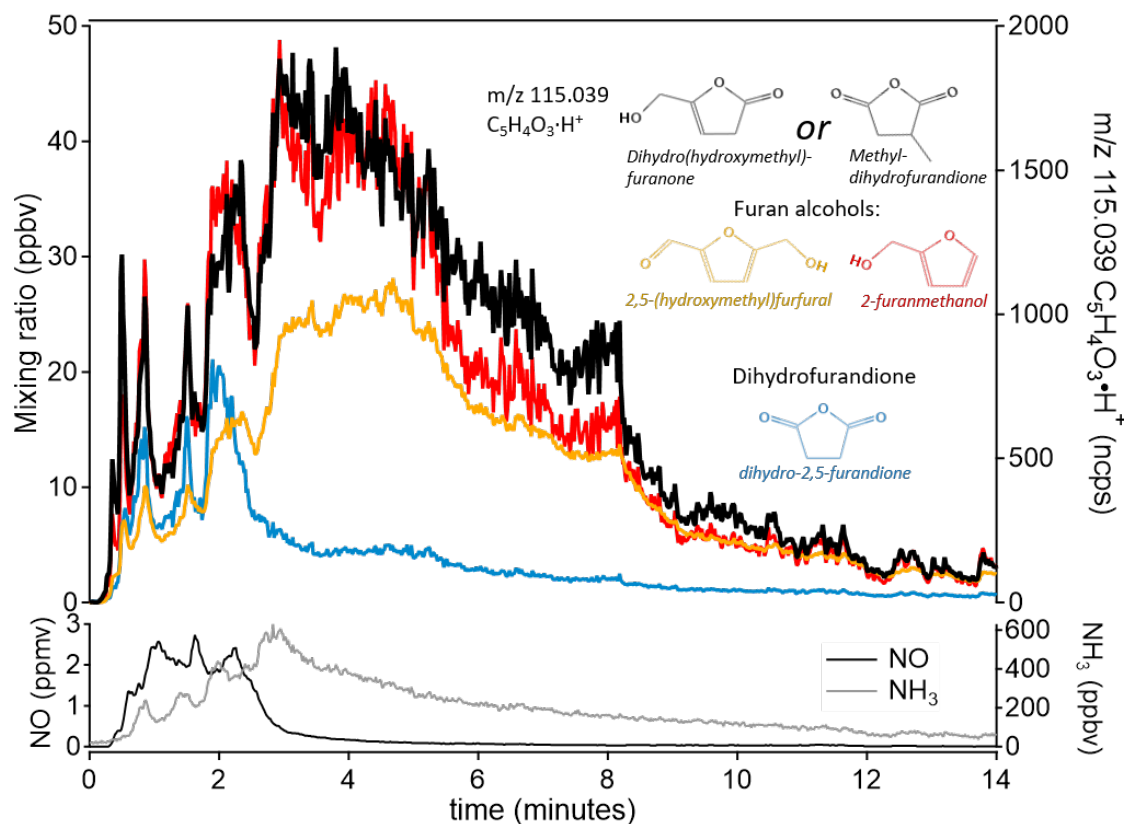
At m/z 115.039 $C_5H_4O_3H^+$ there are several possible candidates with chemical structures similar to species known to be produced by biomass burning. Candidates include furan alcohols and methyldihydrofuran. The time series trace of m/z 115.039 during a ponderosa pine fire (Fire 2) is shown in black and compared to the time series of two furan alcohols: 2,5-(hydroxymethyl)furfural (yellow) and 2-furanmethanol (red); and to dihydro-2,5-furandione (blue). The identities of the furan alcohols and dihydro-2,5-furandione were confirmed through other methods. The superior correlation with furan alcohols is evidence that m/z 115.039 is more likely a furan alcohol than a dione (see text). NO and NH_3 are shown as a reference for higher- and lower- temperature fire processes, respectively. NO described by Stockwell et al., 2017. NH_3 from PTR-ToF.

Atmospheric
Chemistry
and Physics
Discussions

Figure 4
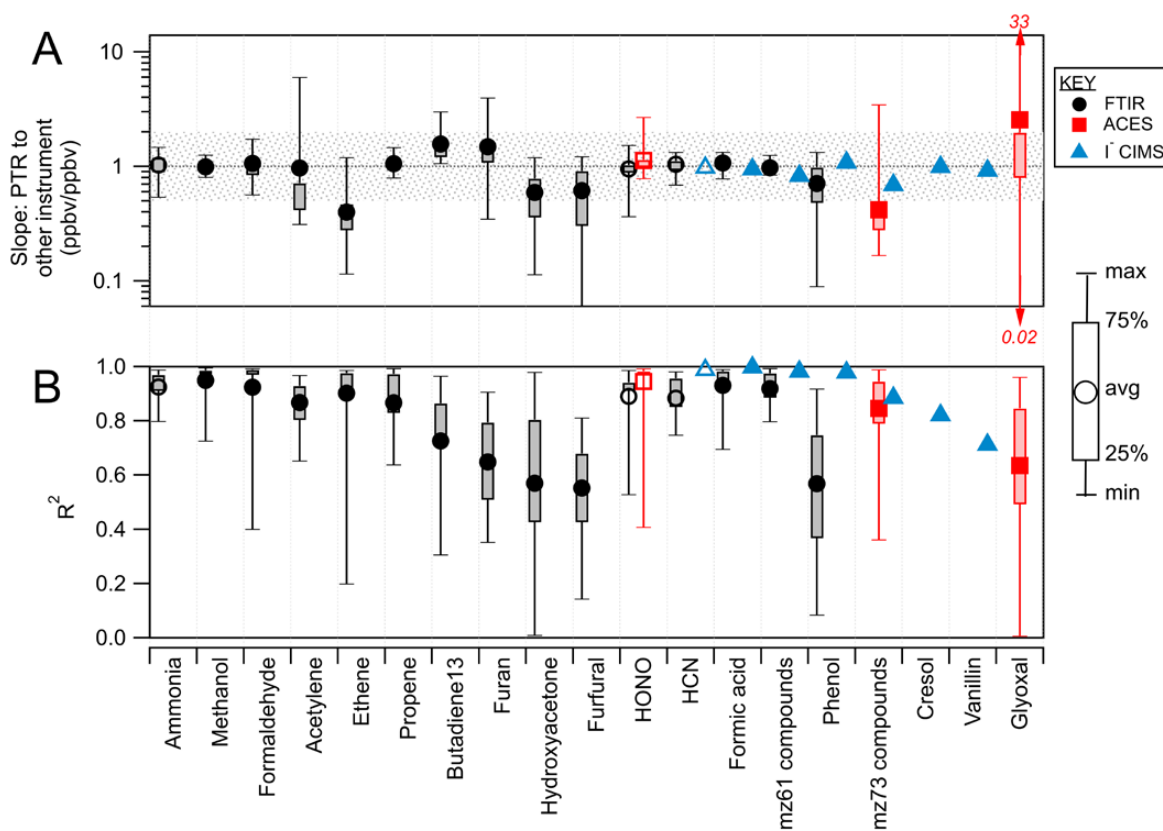
(A) Slope of PTR-ToF measurement compared to other instruments for all stack burns (eighteen fuels). The open symbols indicate that PTR-ToF calibration factors for ammonia, HCN and HONO were determined from the comparison with FTIR during Fire 72 (Ponderosa pine). The shaded area shows a factor of 2. (B) R^2 between PTR-ToF and other instruments. For "hydroxyacetone", the PTR-ToF total mass 75.044 $C_3H_6O_2H^+$ (sum of methylacetate, ethylformate, hydroxyacetone) is compared to FTIR hydroxyacetone. For "mz 61 compounds", the PTR-ToF total mass 61.028 $C_2H_4O_2H^+$ (sum of acetic acid and glycolaldehyde) is compared to the FTIR sum of glycolaldehyde and acetic acid, and I⁻ CIMS acetic acid. For "mz 73 compounds", the PTR-ToF total mass 73.028 $C_3H_4O_2H^+$ (sum of methylglyoxal and acrylic acid) is compared to I⁻ CIMS acrylic acid and ACES methyl glyoxal. For "cresol", the PTR-ToF total mass 109.065 $C_7H_8OH^+$ (sum of anisol and cresol) is compared to I⁻ CIMS cresol. Methanol, formaldehyde, propene, furan, furfural, formic acid, acetic acid, phenol, anisol, and cresol were calibrated directly on PTR-ToF and have an uncertainty of 15%. Ethene and acetylene were also directly calibrated, but are less certain

Atmospheric
Chemistry
and Physics
Open Access
Discussions
EGU

due to variability in O_2^+. 1,3-butadiene, methylacetate, ethylformate, hydroxyacetone, glycolaldehyde, methylglyoxal, acrylic acid, and glyoxal were calibrated using calculation, have an uncertainty of 50%, and represent the lower bound of concentration.

Figure 5
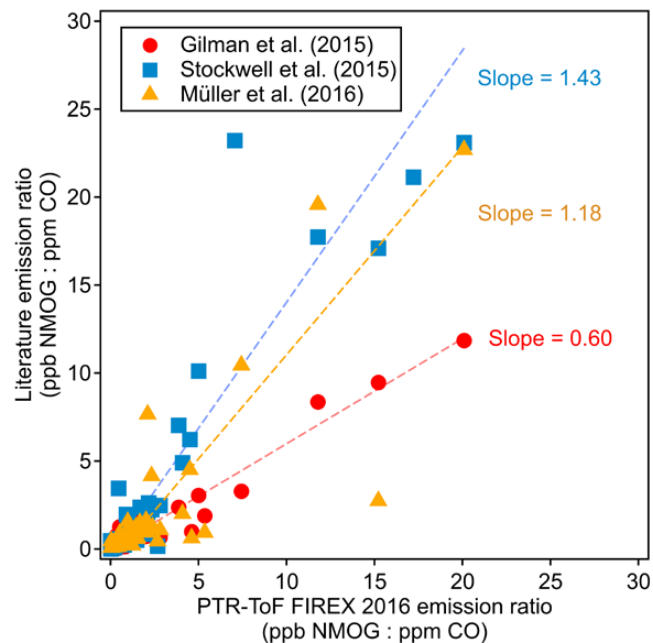
Comparison of emission ratios (ppb NMOG : ppm CO, fire-integrated) between this work and several previously published studies. The emission ratios shown are various NMOGs averaged over all the fires and fuel types reported in each study.

Figure 6
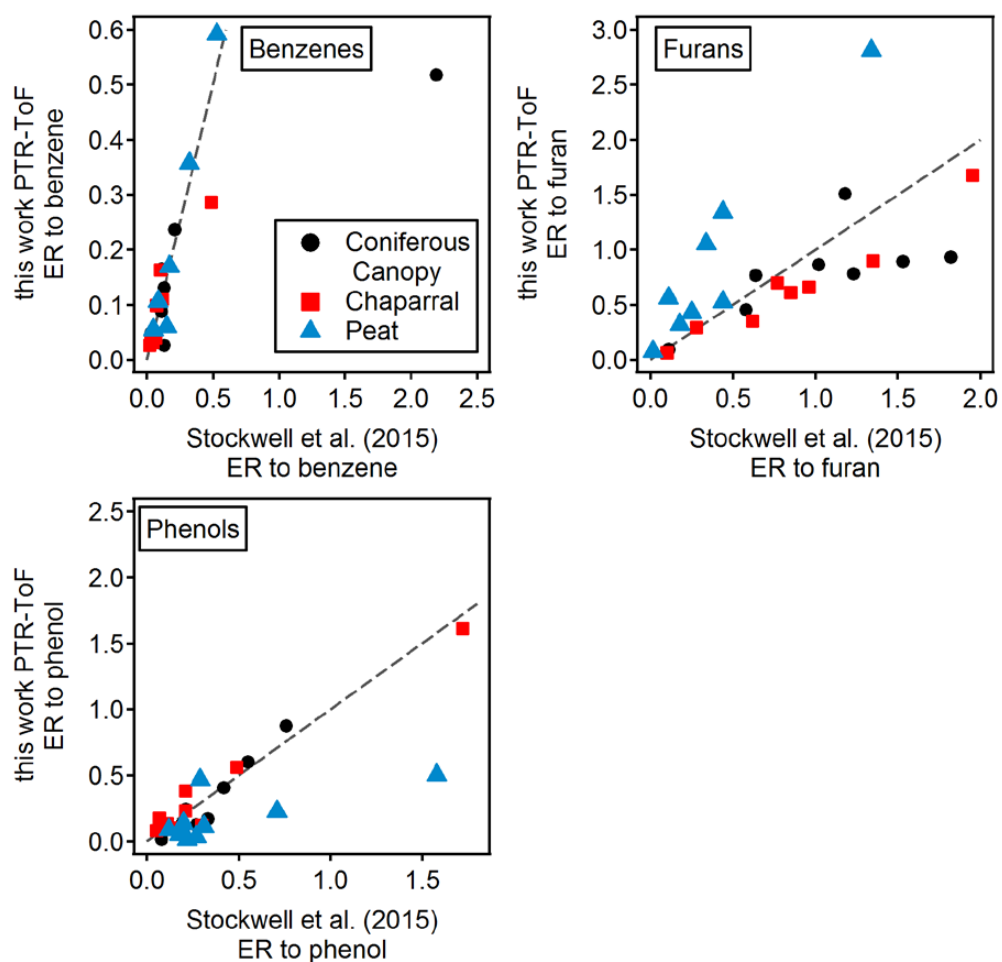
Comparison of emission ratios to Stockwell et al. (2015). The dashed line in each panel shows a 1:1 line. The NMOGs are divided into three structural classes: benzenes, furans, and phenols. In each class, the emission ratio is taken against benzene, furan, and phenol, respectively. Three types of fuels (coniferous canopy, chaparral, and peat) were sampled in both this work and Stockwell et al. (2015) and the data shown are averaged over all the fires of a particular fuel type.

Figure 7
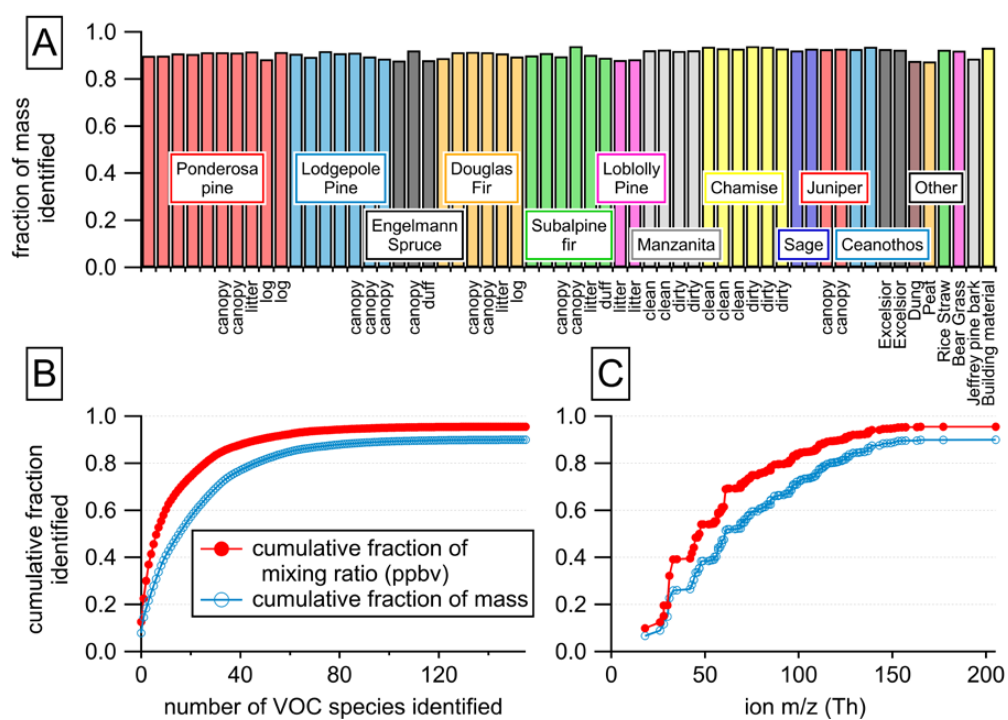
(A) Fraction of detected NMOG mass accounted for by identified species. (B) The fraction of total detected NMOGs accounted for by identified species increases as additional ion masses are interpreted. (C) Identified fraction of total detected NMOG as a function of m/z. Subplots B and C use data from Fire 2 (Ponderosa Pine with a realistic blend of fuel components).

Atmospheric
Chemistry
and Physics
Discussions

Figure 8
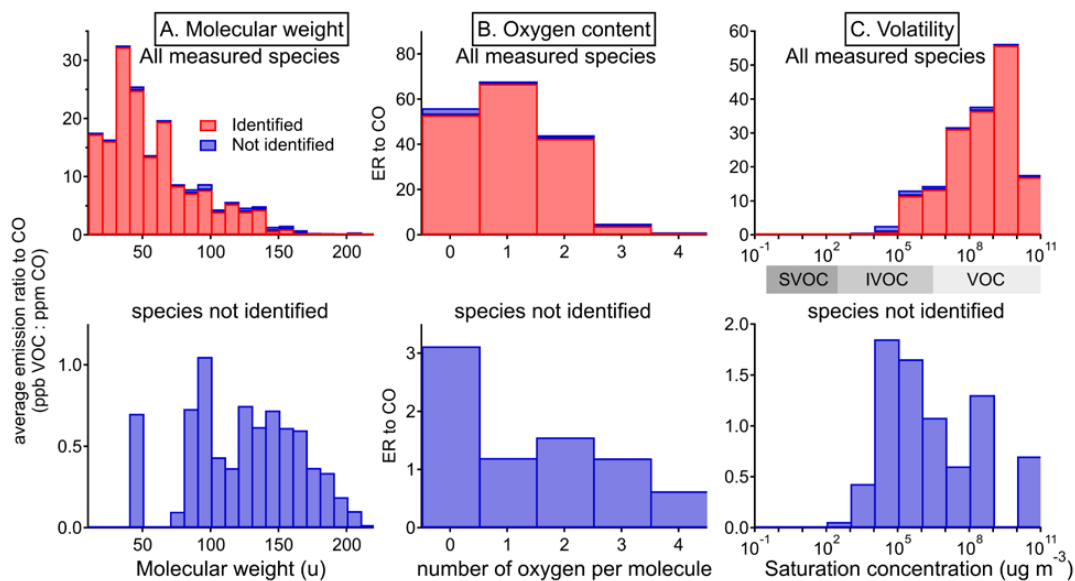
Histogram of total emission (quantified as emission ratio to CO) of identified and unidentified NMOGs, sorted by (A) molecular weight, (B) number of oxygen per molecule, (C) saturation vapor concentration (C_0 at 25ºC). The saturation concentrations are from the CRC Handbook, NIST Chemistry WebBook, and Yaws (2015) where available, and estimated from the parameterization in Li et al. (2016) otherwise.

Figure 9
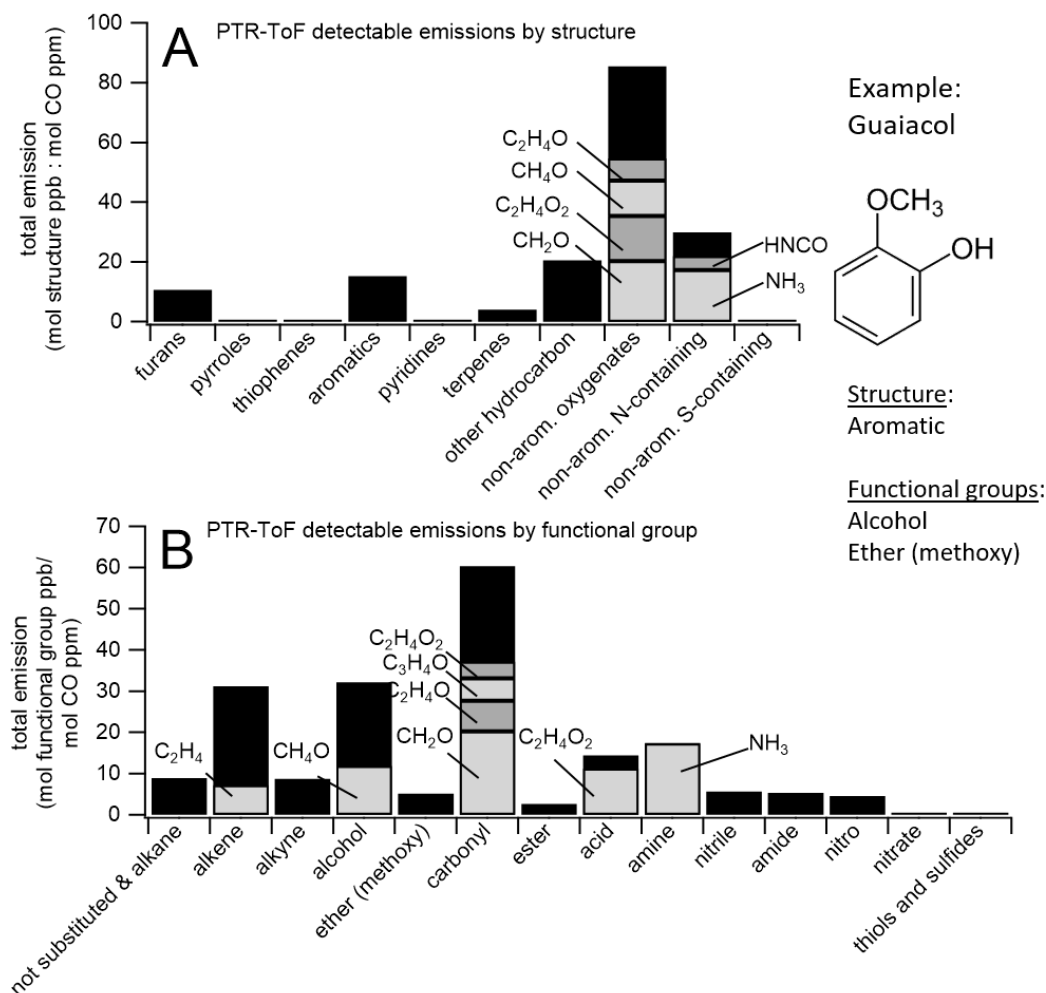
(A) Relative abundance of NMOGs detected by PTR-ToF, sorted by structural category. The abundance is given relative to CO (emission ratio = integrated mmol NMOG/integrated mol CO). (B) Relative abundance of NMOGs (emission ratio to CO), sorted by functional group. Some NMOGs, such as guaiacol, have multiple functional group substitutions. These are counted once in each relevant category. The contributions from several compounds with high concentrations are indicated separately.

Figure 10
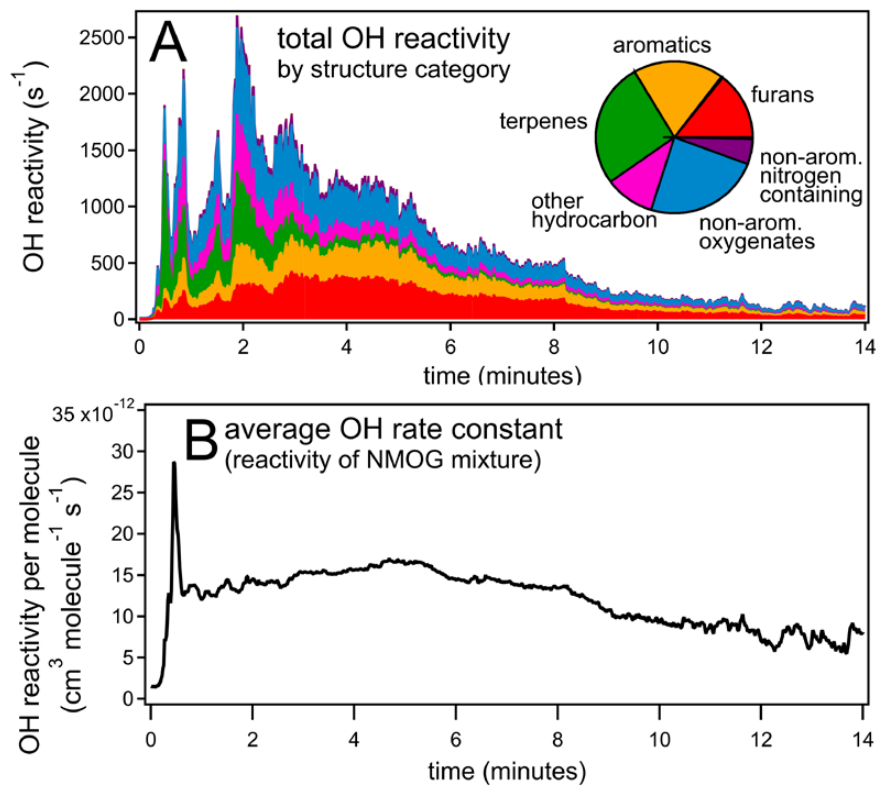
(A) Total OH reactivity from NMOGs measured by PTR-ToF during Fire 2 (Ponderosa Pine). The inset pie chart shows the relative contribution to total OH reactivity of each structural category, averaged over all fires during FIREX 2016. (B) Average rate constant with OH of NMOGs detected by PTR-ToF during Fire 2.

Figure 11
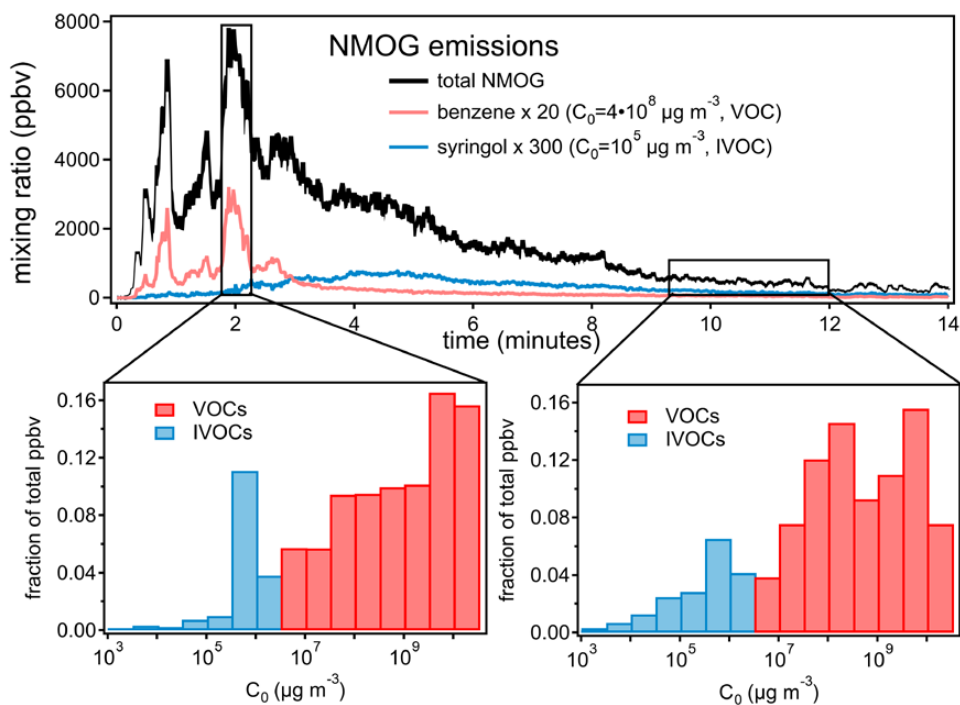
Volatility of NMOGs during Fire 2 (Ponderosa Pine). For simplicity, ammonia is excluded from this figure because of its very high concentration (600 ppb) and volatility ($C_0 = 7 \times 10^9$ µg m^{-3}).